Palaeogeography, Palaeoclimatology, Palaeoecology 683 (2026) 113418

Contents lists available at ScienceDirect

Palaeogeography, Palaeoclimatology, Palaeoecology

journal homepage: www.elsevier.com/locate/palaeo

Brachiopod giants from the Mississippian (Asbian) of western Ireland: Fossil bioarchives of seasonality and symbiosis and far-field harbingers of climate change☆

Lucia Angiolini [a], Karem Azmy [b], Enrico Cannaò [a], Gaia Crippa [a], Eamon Doyle [c], Giovanna Della Porta [a], John Murray [d], Michael O'Connell [e], Marco Viaretti [a], David A.T. Harper [f,*]

[a] Dipartimento di Scienze della Terra "A. Desio", Università degli Studi di Milano, Milan, Italy
[b] Department of Earth Sciences, Memorial University of Newfoundland, St. John's, NL A1B 3X5, Canada
[c] Burren and Cliffs of Moher UNESCO Global Geopark, Clare County Council, Ennistymon, County Clare, Ireland
[d] Earth and Ocean Sciences, School of Natural Sciences, University of Galway, Galway, Ireland
[e] Mainistir, Inishmore, Aran Islands, Co. Galway, Ireland
[f] Department of Earth Sciences, Durham University, Durham DH1 3LE, UK

ARTICLE INFO

Editor: Howard Falcon-Lang

Keywords:
Gigantoproductus
Carbonate facies
Isotopes
Late Palaeozoic climate
Western Ireland

ABSTRACT

Brachiopod species of *Gigantoproductus* have long fascinated researchers, not only because of their exceptional size and thick shell, but also as unparalleled bioarchives for palaeoecological and palaeoclimatic information. In this paper, we describe faunas containing *Gigantoproductus semiglobosus* from upper Visean (upper Asbian) successions in two regions of western Ireland, and report geochemical analyses that improve understanding of the palaeobiology of these brachiopods. The two regions are the Burren, where the Aillwee Member (Burren Formation) comprises thick-bedded cyclic bioclastic packstone to grainstone, interpreted as the deposits in predominantly shallow-water (subtidal) marine environments with episodic subaerial exposure, and the Aran Islands, where the Slievenaglasha Formation comprises cyclic crinoidal limestones with chert, deposited in slightly deeper water conditions. Shallowing upward fourth-order cycles in both regions have previously been interpreted as being under a glacioeustatic control. Reconstructed $\delta^{13}C_{org}$ and $\delta^{15}N_{org}$ of soft tissues of *G. semiglobosus* are respectively −29.0 to −30.1 ‰ (VPDB) and − 1.4 ‰ and + 6.1 ‰ (Air) and serve as proxies for identifying photosymbiotic relationships and a mixotroph lifestyle for this species. Well-preserved $\delta^{18}O_{carb}$ profiles record high seasonal variations ($\Delta\delta^{18}O$ = 0.9 to 1.9 ‰ corresponding to a ΔT = 4 to 11 °C) for palaeoequatorial settings as a far-field proxy of the onset of sustained Gondwanan glaciation in the late Visean and provide evidence of warm tropics during the glaciation. The $\delta^{13}C_{carb}$ profiles are mostly controlled by local influences and changes in productivity. Our geochemical analyses of growth patterns, seasonal variation, diet and endosymbiosis in *G. semiglobosus*, sheds new light on the paradox of these unusual brachiopods, and provides a greater understanding of their massive size.

1. Introduction

The Brachiopod tribe Gigantoproductini has always represented a challenge to researchers because of their large size and thick shells, which have no analogues in living faunas, and more generally across the entire brachiopod phylum. The reasons for unusual morphologies and occurrences, particularly during the Mississippian, are still an issue of debate. Few studies have provided any concrete solutions (e.g., Angiolini et al., 2019). Size increase in invertebrate groups has been attributed to greater oxygen availability, increased primary productivity, and predation pressure (Zhang et al., 2015), although competition may have played a more central role than predation in driving gigantism (Vermeij, 2016). Gigantism is commonly linked to high metabolic rates and often associated with symbiotic relationships, which enhance metabolic

☆ This article is part of a Special issue entitled: 'Brachiopods' published in Palaeogeography, Palaeoclimatology, Palaeoecology.

* Corresponding author.
E-mail address: david.harper@durham.ac.uk (D.A.T. Harper).

https://doi.org/10.1016/j.palaeo.2025.113418
Received 20 September 2025; Received in revised form 10 November 2025; Accepted 10 November 2025
Available online 12 November 2025

activity and promote skeletal growth through calcification (Cowen, 1983; Key Jr et al., 2005). The large size of some Permian brachiopods, such as lyttonioids and richthofenioids, may be related to tropical habitats and possible symbiosis with zooxanthellae (Cowen, 1970), while others, like *Peregrinella,* may have exploited chemosymbiotic diets (Campbell and Bottjer, 1995; Posenato and Morsilli, 1999; Kiel et al., 2014). In contrast, some gigantism occurred under low-resource conditions, with low metabolic rates and slow growth, a phenomenon known as the "gentle giant syndrome" (Rosa and Seibel, 2010; Vermeij, 2016).

Angiolini et al. (2019) attributed the gigantic size and thick carbonate shells of some Mississippian species of *Gigantoproductus* from Derbyshire, UK, to a mixotrophic lifestyle, allowing them to obtain energy and nutrients from both photosymbiotic microbes and suspended particulate food. To support this hypothesis, they investigated the carbon and nitrogen isotope composition ($\delta^{13}C_{org}$ and $\delta^{15}N_{org}$) of the organic matter trapped within the shell, a biogeochemical marker indicative of symbiosis (Levin and Michener, 2002; O'Donnell et al., 2003; Mae et al., 2007; Dreier et al., 2012, 2014). Although extracting and analysing shell organic matter is challenging due to its extremely low content, the thick shell of *Gigantoproductus* provides excellent opportunities for such analyses (Angiolini et al., 2019). Similarly, its robust shell serves as a reliable biomineral archive for measuring oxygen and carbon isotopes ($\delta^{18}O$ and $\delta^{13}C$) in calcite (Grossman et al., 2008; Angiolini et al., 2012), offering valuable insights into late Palaeozoic climate and environmental conditions. In particular, $\delta^{18}O$ profiles across the thick calcitic shells allow reconstruction of seasonal variation, as demonstrated by Angiolini et al. (2012). Constraining past seasonality is important, as increased seasonality is often associated with colder conditions and the development of ice accumulations (Ivany et al., 2000; Pross and Klotz, 2002; Steuber et al., 2005; Eldrett et al., 2009; Ferguson et al., 2011; Hennissen et al., 2015; Crippa et al., 2016a; Viaretti et al., 2025), thus providing additional evidence for the timing of the Mississippian phases of the Late Palaeozoic Ice Age (LPIA).

Although the Gigantoproductini from Derbyshire have been intensively studied for these purposes (Angiolini et al., 2012; Nolan et al., 2017; Angiolini et al., 2019), significantly less attention has been devoted to the rich assemblages from Ireland. Brachiopods are locally common in the Mississippian limestones of the Aran Islands and also the Burren region in counties Galway and Clare, respectively, in the west of Ireland, and have been mentioned sporadically since M'Coy's monograph (M'Coy, 1862).

The currently investigated carbon and nitrogen isotope composition of the organic matter trapped in the shell and the oxygen and carbon stable isotope composition of the shell calcite of an upper Visean (Mississippian) species of *Gigantoproductus* from different settings in Ireland confirm that brachiopods are renowned high-resolution archives of climate conditions in the geological past. Furthermore, the study of their microstructure and geochemistry provides insights into growth pattern, reveals trophic strategies and allows the reconstruction of past seasonal variations during critical time intervals of global change.

2. Geographic and geological setting

The Carboniferous rocks of the Shannon Basin are spectacularly exposed on the western seaboard of Ireland (Fig. 1). Mississippian strata crop out on the Burren (County Clare) and on the Aran Islands (County Galway) as part of the broader Galway-Roscommon Shelf (Sevastopulo and Wyse Jackson, 2009). This thick carbonate succession was deposited on the platform adjacent to a long-lived intracratonic depocenter located farther south during the Tournaisian and Visean (Strogen, 1988; Somerville and Strogen, 1992; Strogen et al., 1996; Murray, 2010; Somerville et al., 2011). Marked sedimentary cyclicity is conspicuously developed in the upper Visean part of the succession (Asbian and Brigantian regional substages). In the Burren, this interval lithostratigraphically corresponds to the Burren and Slievenaglasha formations (Figs. 2–3).

The Burren Formation consists of c.356–386 m of pale grey, shallow marine skeletal carbonates (Pracht et al., 2004; Gallagher et al., 2006). The uppermost c.152 m is termed the Aillwee Member and consists of nine prominent shallowing-upwards cycles of thick skeletal limestones, which have palaeokarstic tops and are commonly capped by thin non-calcareous clay horizons (Gallagher, 1996). This feature of the bedrock has resulted in the distinctive scarp and terrace morphology of the Burren landscape, with each cycle or 'terrace' in the stratigraphy labelled T1-T9 (from oldest to youngest; see Fig. 2).

Gallagher et al. (2006) noted a late Asbian age (Cf6γ foraminifer zone of Conil et al., 1991; equivalent to MFZ14 of Poty et al., 2006) for the Aillwee Member, with T1–7 and T8–9 representing the Cf6γ1 and Cf6γ2 subzones, respectively (Fig. 2). These authors also noted the first

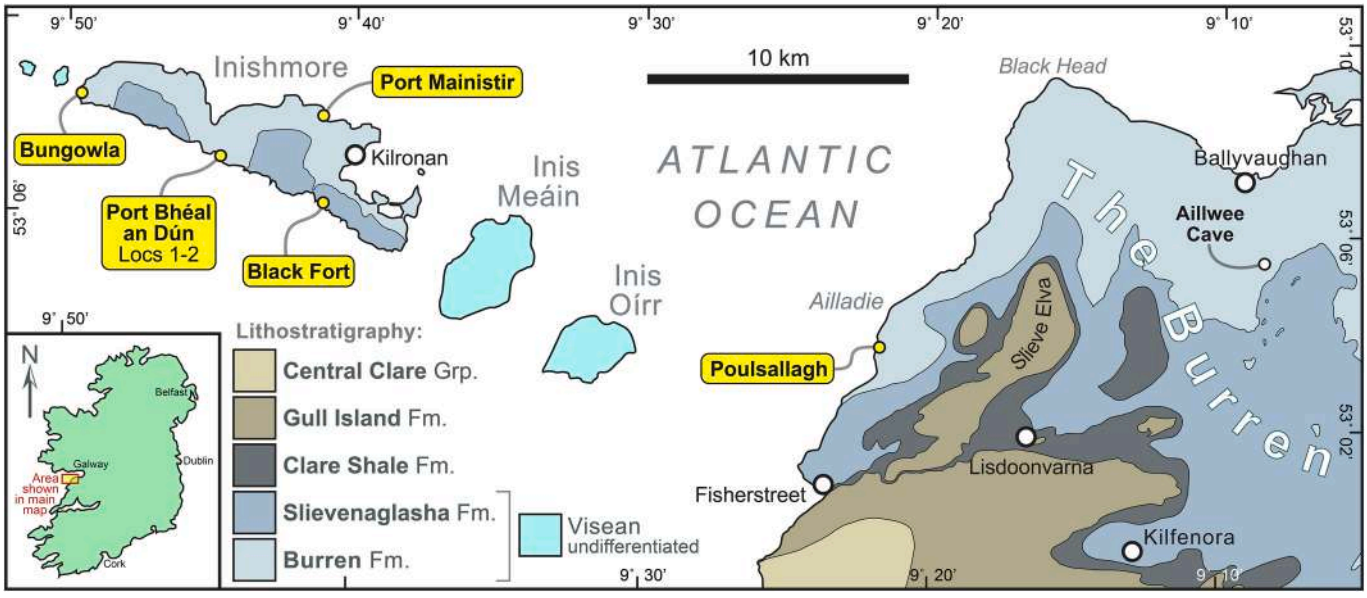

Fig. 1. Location of study area. Main map shows summary Carboniferous geology and sample locations (yellow filled circles) in the Burren region of north Clare and Aran Islands. Inset map (bottom left) shows location of study area in western Ireland. Geological map adapted from Geological Survey Ireland data. (For interpretation of the references to colour in this figure legend, the reader is referred to the web version of this article.)

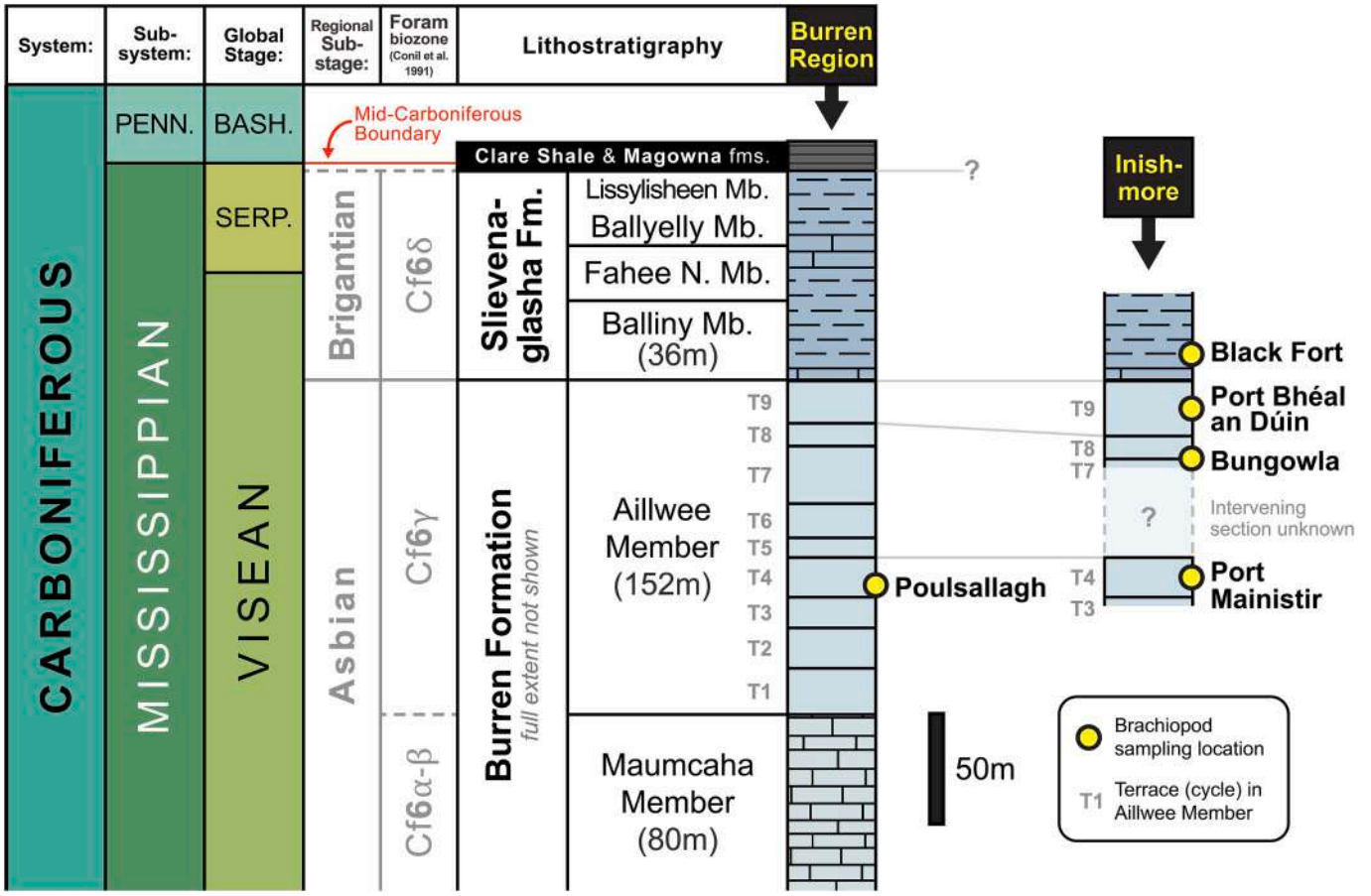

Fig. 2. Summary Mississippian stratigraphy for the Burren region and Inishmore (Aran Islands). Note the cyclic terraces (T1-T9) in the Ailwee Member and approximate lithostratigraphic position of the various sample locations (yellow filled circles). (For interpretation of the references to colour in this figure legend, the reader is referred to the web version of this article.)

appearance of the upper Asbian brachiopod *Davidsonina septosa* (Phillips, 1836) in T4 of the Aillwee Member, and the first appearance of the Brigantian taxon *Gigantoproductus edelburgensis* (Phillips, 1836) just below the very top of the Burren Formation. The upper part of the Aillwee Member also crops out on Inishmore, with T8–9 impressively exposed in the cliff sections on the southwest coast of the island. A complete vertical transect through T9 is present at Port Bhéal an Dúin, where it is 25 m thick and composed of medium grey skeletal packstones, which are locally rich in calcareous algae (Somerville, 1999; Pracht et al., 2004). The foraminiferal fauna recorded from this particular location by Somerville (1999, p.106) included the key diagnostic taxa *Bradyina rotula* (Eichwald, 1859), *Asteroarchaediscus* sp. and the calcareous alga *Saccaminopsis* sp., indicating a latest Asbian (Cf6γ2b-c) age. These taxa are also known to extend up into the lower Brigantian regional substage.

The Burren Formation is overlain by the Slievenaglasha Formation, which consists of 95 m of cyclic crinoidal limestones. It was deposited in a shallow subtidal open marine environment, possibly in slightly deeper-water conditions than the underlying Burren Formation (Gallagher, 1996; Gallagher et al., 2006; Sevastopulo and Wyse Jackson, 2009). This platform-wide deepening during the Brigantian Age caused deeper-water shelf subtidal chert-rich limestone to be deposited across Ireland. Sediment cycles and shoaling are evident in the Slievenaglasha Formation, but evidence for subaerial exposure is generally lacking, except for a prominent palaeokarst at the top of the unit (Gallagher et al., 2006; Doyle et al., 2021). Gallagher et al. (2006) proposed a Cf6δ (= lower part of MFZ15) subzone age for the Slievenaglasha Formation. Somerville (1999) noted a similar Brigantian foraminiferal subzone age for the unit on Inishmore. Conodonts recovered from the very top of the formation indicate that it extends up into the Serpukhovian (Barham et al., 2015; see also Cózar and Somerville, 2021; Fig. 2).

The cyclicity evident in the Burren and Slievenaglasha formations in western Ireland is also observed regionally elsewhere in Ireland (e.g., Gallagher, 1996) and Britain (e.g., Wright and Vanstone, 2001) and has been interpreted as glacio-eustatically driven, coincident with the onset of the Late Palaeozoic Ice Age (e.g., Soreghan and Giles, 1999; Wright and Vanstone, 2001; Fielding et al., 2008; Rygel et al., 2008; Barham et al., 2012; Fielding, 2021).

In the Shannon Basin, a pronounced basin-wide shift to non-calcareous terrigenous sedimentation occurred during the Serpukhovian (Sevastopulo, 2009; Murray, 2010). In the Burren, the Slievenaglasha Formation is overlain by a very thin unit of dark argillaceous limestones and shales (Magowna Formation), followed by dark organic-rich shales with a predominantly pelagic fauna (Clare Shale Formation) (Pracht et al., 2004). O'Sullivan et al. (2021) produced a U-Pb date of 320.7 ± 2.0 Ma from early diagenetic phosphate from the base of the Clare Shale Formation, indicating a Bashkirian Age.

3. Material and methods

3.1. Sample localities and repository

Specimens of the Visean species *Gigantoproductus semiglobosus* (Paeckelmann, 1931) were collected from several sites in the Burren and Inishmore (see Table 1 for details). Their geographical location and relative stratigraphic positions are shown in Figs. 1–2 and field photographs of the sampling localities are presented in Fig. 3. During the Early Mississippian, Ireland was located south of the palaeoequator in tropical

Fig. 3. Field photos of sampled sites in the Burren and on the Aran Islands. a. Limestone platform on shore at Poulsallagh, Aillwee Member Terrace 4, Burren Formation; b, c. Quadrat sampling on shore at Port Mainistir, Lower Aillwee Member Terrace 4, Burren Formation; d, e, development of shell beds in vertical and f, horizontal views, Port Bhéal an Dúin, Aillwee Member Terrace 9, Burren Formation; g, Black Fort, Slievenaglasha Formation.

latitudes (Rowley et al., 1985; Blakey, 2008; Barham et al., 2012, see Fig. SM1 palaeogeographic map in supplementary material).

All the analysed specimens are housed in the collections of the Dipartimento di Scienze della Terra 'A. Desio' of the University of Milan, and registered with reference numbers consisting of a prefix MPUM followed by a five-digit number. Two specimens from BU2 (MPUM13528–13529) and two from AR10 (MPUM13534–13535), and one each from AR2 (MPUM13532) and AR11 (MPUM13536–13538) were analysed for geochemistry. The other specimens were used for taxonomic identification, microstructural study, and palaeoecological interpretation.

3.2. SEM analysis

Brachiopod specimens were cut in half sagittally from the umbo to the anterior commissure along the axis of maximum growth using a low-speed saw with a thin diamond blade. Sectioned shells were observed on acetate peels and investigated in thin section, together with cathodoluminescence and the Scanning Electron Microscope (SEM). For SEM analyses, shell sections were prepared following the method of Crippa et al. (2016b). Sections were ground smooth using silicon carbide (SiC) powder of two different granulometries, etched with 5 % hydrochloric acid (HCl) for 10 s to reveal the details of the microstructure, and washed with demineralised water. The prepared surfaces were then coated with gold and observed under a JEOL JSM-IT500 LA SEM at the University of Milan.

3.3. Petrographic and CL analyses

Petrographic analysis of thin sections to inspect the brachiopod shells and the texture and composition of the surrounding and internal deposits was performed using a Zeiss polarized light microscope

Table 1
Brachiopod sample localities.

Sample Number:	Museum number:	Site location:	Region:	Grid reference:	Formation:	Comments:	Geochemical analyses
AR11	MPUM13536–13538	Black Fort	Inishmore	N53°06′18,2" W9°41′12,1"	Slievenaglasha Formation		O, C isotopes and TE (MPUM13536); N isotopes (MPUM13537, MPUM13538)
AR10	MPUM13533–13535	Port Bhéal an Dúin		N53°07′07,6" W9°44′43,1"	Burren Formation	Aillwee Member Terrace 9	O, C isotopes and TE (MPUM13534, MPUM13535)
AR12	MPUM13539–13540	Bungowla		N53°08′20,6" W9°49′35,1"		Aillwee Member Terraces 7–8	–
AR1–**AR2**	MPUM13531–13532	Port Mainistir		N53°08′02,1" W9°41′08,5"		Lower Aillwee Member Terrace 4	O, C isotopes and TE (MPUM13532)
BU2	MPUM13528–13530	Poulsallagh	Burren region	N53°03′33,5" W9°21′47"		Aillwee Member Terrace 4	O, C isotopes and TE (MPUM13528, MPUM13529); N isotopes (MPUM13528)
BU1	MPUM13521–13527	Aillwee Cave		N53°05′22,7" W9°08′35,9"		Aillwee Member Terrace 1	–

equipped with a digital camera on four thin sections from Burren (MPUM13522, MPUM13527, MPUM13529, MPUM13530) and five thin sections from Inishmore (MPUM13532, MPUM13534, MPUM13535, MPUM13536, MPUM13539). All thin sections were also examined under cathodoluminescence microscopy with a Cambridge Image Technology Limited (CITL) luminoscope (model MK 5–2 operating system at 10–16 kV with a beam current between 200 and 400 μA, and vacuum gauge 50–70 mTorr).

3.4. In-situ minor and trace element analyses of carbonate shell

Minor and trace elements were measured in situ at each spot analysed for stable isotopes, to assess shell preservation. The in-situ minor and trace element compositions of carbonate shells were determined using a laser ablation system (Teledyne Photon Machines) coupled with a single-collector quadrupole ICP-MS (iCAP RQ, Thermo Fisher Scientific) housed at the Geochemistry, Geochronology and Isotope Geology Laboratory at the Dipartimento di Scienze della Terra "A. Desio", University of Milan. The laser ablation system is an Analyte Excite 193 nm ArF excimer laser microprobe equipped with HelEx II volume sample chamber for fast wash out. The instrument was tuned for robust plasma conditions by optimising the laser and the ICP-MS settings and monitoring the $^{232}Th^{16}O^{+}/^{232}Th^{+}$ below 0.3 % and the $^{238}U^{+}/^{232}Th^{+}$ at ca. 1.1 while ablating the NIST SRM 610 in line scan mode. Analyses were conducted using a beam diameter of 85 μm, a laser pulse frequency of 10 Hz and a laser energy density of ~ 8.6 J/cm^2. Ablated particles were transported to the ICP-MS using a PTFE tubing with He gas at a flow rate of 0.54 and 0.36 l/min into the sample chamber and in the HelEx II cup, respectively. Each spot was analysed for a total of 90s, which included 40s of background analysis (comprising 10s of laser warm up), 40s of laser ablation measuring isotope peak intensity, followed by 10s of wash out time. The soda-lime glass NIST SRM 610 (Jochum et al., 2011) was used as an external standard, whereas ^{43}Ca was selected as an internal standard. Quality control was achieved by analysing carbonate nanopellets MACS-3NP and NHFS-2-NP (Jochum et al., 2019; Boer et al., 2022) and calcite UWC-3 (Orland et al., 2014) (Supplementary Table S1). The software Glitter (Griffin et al., 2008) was used for data reduction with the linear fit-to-ratio method, and the signals were filtered for spikes on an element-by-element basis. Determined concentrations were further filtered to eliminate values too close to the detection limit (value – 2 standard deviation > detection limit). Precision is evaluated as the relative standard deviation (1RSD%) whereas accuracy is evaluated as the relative deviation from the reference values. Both are commonly better than 10 % for most of the trace elements with concentration approaching 1 μg/g (Supplementary Table S2). Laser ablation pits were positioned close to the areas microdrilled for stable isotopes, avoiding broken surfaces compromised by the microdrilling (Supplementary Fig. S1). The time-resolved spectra were carefully evaluated, taking into account all potential factors influencing the trace element budget (e.g., presence of inclusions), dissimilar to the intrinsic vital effect of the carbonate shell (e.g., variation in Ba content). Reported LA-ICP-MS spot analyses are correlated with the corresponding single stable isotope data.

3.5. C and N isotopes from the shell organic fraction

Carbon and nitrogen isotope ratios of the organic fraction were measured on shells MPUM13528, MPUM13537, and MPUM13538 in the isotope laboratory of the Department of Earth Sciences at Memorial University of Newfoundland, St. John's, Canada. Due to the very low contents of organic matter, approximately 50 g of powder was obtained from six brachiopod specimens. The samples were digested in 20 % distilled HCl with acid added in 10 ml increments. The samples were stirred after each addition of HCl until there was no visible reaction. After the carbonate reaction was complete, the samples were centrifuged in 50 ml Nalgene centrifuge tubes. The residue was rinsed three times with deionised water using the centrifuge procedure and dried overnight at 40 °C.

Organic carbon- and nitrogen-isotope ratios were measured on the isolated kerogen, using a Carlo Erba Elemental Analyzer coupled to a ThermoFinnigan DELTA V plus isotope ratio mass spectrometer. The results (Table X1) were normalised to the standards IAEA-CH-6 ($\delta^{13}C = -10.4$ ‰ VPDB), NBS18 ($\delta^{13}C = -5.0$ ‰ VPDB), USGS24 ($\delta^{13}C = -16.0$ ‰ VPDB), IAEA-N-1 ($\delta^{15}N = +0.4$ ‰ air), and IAEA-N-2 ($\delta^{15}N = +20.3$ ‰ air). Based on routine repeated measurements of standards, the relative uncertainty (standard deviation divided by the absolute mean) was ~0.2 ‰.

3.6. O and C isotopes from the shell calcite

For sclerochemical analyses, powder samples from the columnar tertiary layer of six shells (Supplementary Table S3) were collected at a high-resolution spacing of ~1 mm using a hand-held microdrill equipped with a 300 μm tungsten carbide drill bit. The columnar tertiary layer was sampled from the posterior to the anterior part, where the entire shell was preserved; the laminar secondary layer was not sampled for geochemical analyses. In one specimen (MPUM13529), the anterior part of the shell was too thin; therefore, we did not sample it in order to avoid mixing with the surrounding matrix. The number of powder samples collected from each specimen was variable, from 35 to 72 samples per shell. Samples were analysed for carbon ($\delta^{13}C$) and oxygen ($\delta^{18}O$) isotope composition using an automated carbonate preparation device

(GasBench II) connected to a Delta V Advantage (Thermo Fisher Scientific Inc., Waltham, Massachusetts, USA) isotope-ratio mass spectrometer (IRMS) at the Dipartimento di Scienze della Terra of the University of Milan. Isotope values ($\delta^{18}O$, $\delta^{13}C$) are reported as per mil (‰) deviations of the isotope ratios ($^{18}O/^{16}O$, $^{13}C/^{12}C$) calculated to the Vienna Pee Dee Belemnite (VPDB) scale using the International Atomic Energy Agency 603 standard (IAEA-603) and NBS-18 standard and within-run internal laboratory standards from Carrara marbles. Analytical reproducibility (1σ) for these analyses was better than 0.1 ‰ for $\delta^{18}O$ and $\delta^{13}C$ values.

Seawater temperature seasonality was calculated from the $\delta^{18}O$ by averaging the differences between the maximum and minimum values of each growth increment ($\Delta\delta^{18}O$), identified between two consecutive growth lines within the columnar tertiary layer of each shell. The position of growth lines within the shell was defined based on observations in peels and thin sections (Supplementary Fig. S2). The same was also done for carbon isotope values ($\Delta\delta^{13}C$). To transform these differences ($\Delta\delta^{18}O$) into seawater temperature (ΔT), we employed the brachiopod-based oxygen-isotope thermometer of Brand et al. (2019), assuming a $\delta^{18}O$ value of 0 ‰ VSMOW for the seawater ($\delta^{18}O_{sw}$) (ΔT_1). However, due to uncertainties related to assumptions about past seawater $\delta^{18}O$ values, we also estimated seasonal palaeotemperature variations from $\Delta\delta^{18}O$ values, considering that a shift of 1 ‰ in $\delta^{18}O$ values corresponds to a temperature change of 4.3 °C (Grossman and Ku, 1986) (ΔT_2). For the discussion, we have considered the mean of ΔT_1 and ΔT_2 in all the analysed shells.

4. Results

4.1. *Gigantoproductus semiglobosus* (Paeckelmann, 1931): systematic notes and depositional environment

The available specimens are characterised by a large size with concave-convex shells and a longitudinally curved profile; the ears are not extended (Fig. 4). The flanks are steep, and the venter convex. The shell substance comprises a thick columnar layer, with a variable thickness exceeding 10 mm in the posterior region, but thinning anteriorly. The ornamentation consists of fine costellae with narrow interspaces, locally sinuous, numbering 11–13 per 10 mm; flutings are absent and poorly developed rugae on the ears and flank; spines are few and scattered. These features, and in particular the variable shell thickness, the longitudinal and transverse profiles, the ribbing, and the absence of fluting, fit well with the description of *Gigantoproductus semiglobosus*.

Although the specimens under examination are often incomplete, they preserve the key morphological traits of the species, allowing for a confident assignment to *G. semiglobosus*. Qiao and Shen (2015) placed the species in the genus *Gigantoproductus*, but Aretz et al. (2019) attributed it to the genus *Datangia*. However, the latter is characterised by the absence of brachial cones and by indistinct brachial ridges, which are instead present in the specimens of *G. semiglobosus* described by Paeckelmann (1931) and Zakowa (1985).

According to Zakowa (1985), the species occurs in the Asbian of England, Belgium, and the Urals and in the Asbian-Brigantian of Poland. According to Qiao and Shen (2015), *G. semiglobosus* ranges up to the lower Serpukhovian. The specimens from the Burren and Inishmore were found in dense assemblages in life-position, with the convex and thick ventral valve down in the substrate and usually with a consistent umbonal orientation (about NE/SW at Port Mainistir).

Microfacies analyses suggest that the depositional environment was a shallow subtidal low to high-energy setting in an inner ramp, in some cases affected by subaerial exposure (Supplementary Table S4).

Samples from the Aillwee Member in the Burren (MPUM13522, MPUM13527, MPUM13529, MPUM13530) are uniform in terms of facies, texture, skeletal grain composition and diagenesis (Fig. 5). They consist of peloidal skeletal packstone to grainstone with abundant

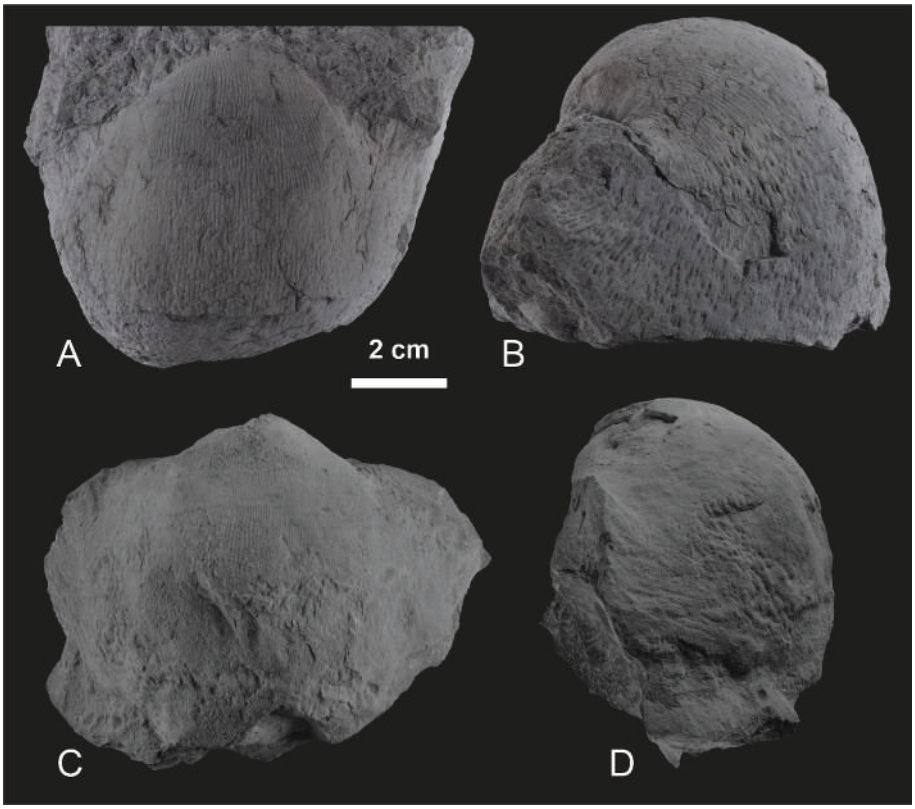

Fig. 4. *Gigantoproductus semiglobosus*. A-B: MPUM13531, A) ventral view of the ventral valve; B) lateral view of the ventral valve. C-D: MPUM13526, C) ventral view of the ventral valve; D) lateral view of the ventral valve.

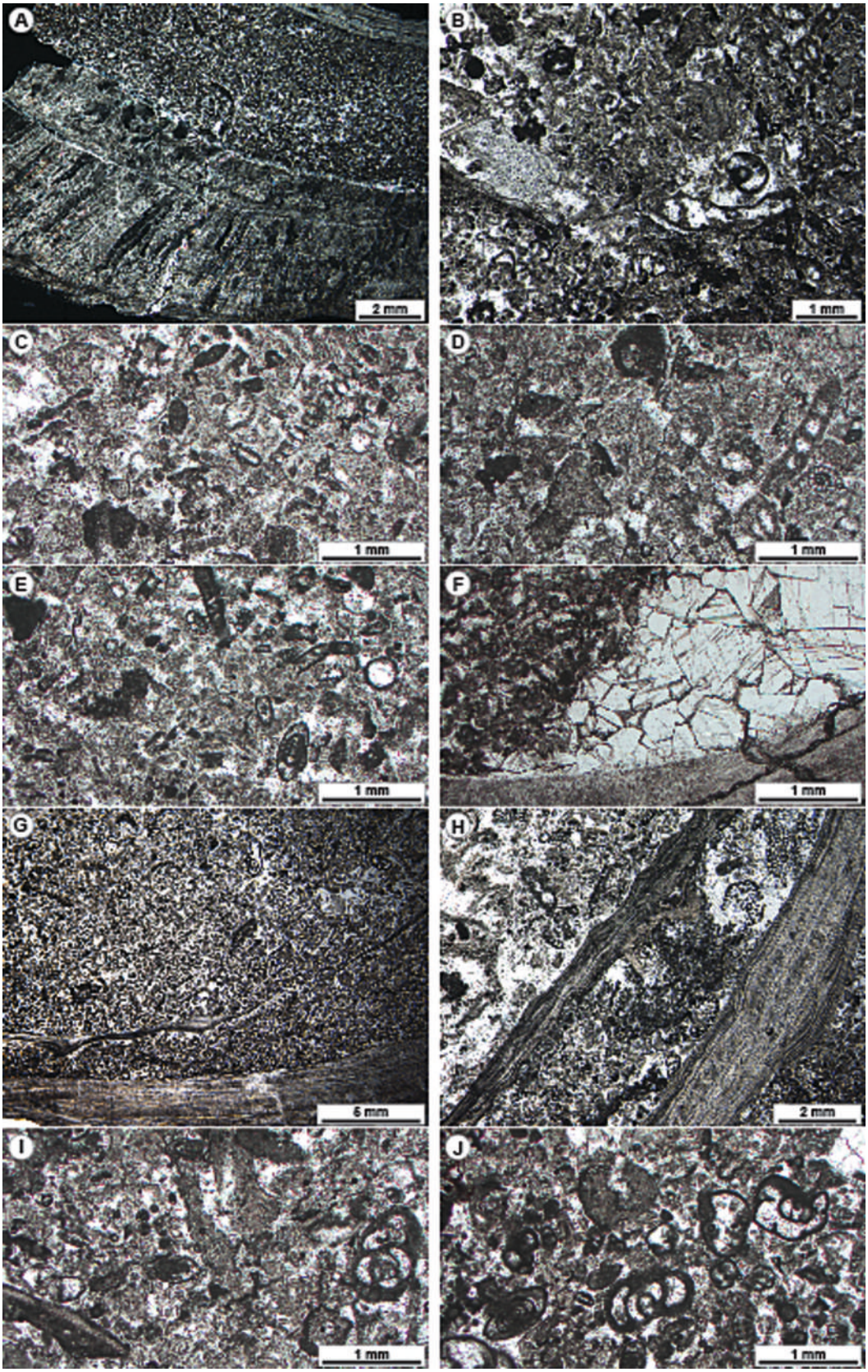

(caption on next page)

Fig. 5. Microfacies of the Burren Formation in the Burren Region. A) Photomicrograph in crossed polarisers showing the brachiopod shells and the sediment infill of peloidal skeletal packstone (sample MPUM13527). B) Peloidal skeletal packstone to grainstone including fragments of red alga *Fasciella*, green algae palaeoberesellids, crinoid ossicles and benthic foraminifer as *Earlandia vulgaris* and endothyrids (sample MPUM13522). C) Skeletal packstone to grainstone with a fragment of the dasyclad *Koninckopora* associated with *Tuberitina* and endothyrid foraminifers (sample MPUM13522). D) Skeletal packstone to grainstone with red algae *Fasciella*, palaeoberesellid algae and endothyrid foraminifers (sample MPUM13522). E) Skeletal packstone to grainstone with red algae *Fasciella*, calcispheres, endothyrid and eostaffellid foraminifer (sample MPUM13522). F) Geopetal filling in brachiopod shell with skeletal packstone below (left) and burial equant drusy cement above (right) (sample MPUM13527). G) Panoramic photomicrograph showing the brachiopod shells and the infilling and surrounding skeletal peloidal packstone (sample MPUM13529). H) Calcareous algae are common in the internal and surrounding skeletal packstone: *Koninckopora*, palaeoberesellids and *Fasciella* (sample MPUM13530). I) Packstone with micrite coated skeletal grains, common *Fasciella* and *Omphalotis* endothyrid foraminifers (sample MPUM13529). J) Abundant endothyrid and eostaffellid foraminifers associated with red alga *Fasciella* (sample MPUM13529). (For interpretation of the references to colour in this figure legend, the reader is referred to the web version of this article.)

peloids, sparse green calcareous algae as the palaeoberesellids and dasyclad algae as *Koninckopora*, associated with sparse red algae as *Fasciella*. Benthic foraminifers vary from rare to common and include endothyrids, palaeotextulariids, eostaffellids, *Bradyina*, *Tuberitina* and *Earlandia vulgaris* (Rauzer-Chernousova and Reitlinger, 1937). Calcispheres are commonly associated with sparse ostracods, rare crinoid ossicles, brachiopod fragments, bivalves, rugose and auloporid corals and fenestellid bryozoans. Texture and composition are indicative of a lagoonal environment, low to moderate energy, within the photic zone and open marine. The diagenetic features reflect marine biogenic micritisation, phreatic meteoric cementation through non-luminescent equant to scalenohedral sparite; micrite matrix recrystallisation in blotchy luminescent microsparite; burial cementation by dull luminescent blocky and drusy calcite cement surrounded by bright luminescent inter-crystal overgrowth.

The samples from Inishmore are diverse in terms of lithofacies and skeletal composition (Figs. 6–7). The microfacies associated with specimen MPUM13532 (Port Mainistir) represents a subtidal low-energy, restricted lagoon affected by subaerial exposure with palaeosol development at the top of shallowing-upward glacio-eustatic cyclothems. The sediment surrounding and filling the brachiopod shell is a peloidal skeletal packstone to wackestone with common fragments of palaeoberesellid algae, calcispheres, sparse endothyrids affected by dissolution vugs, pendant vadose and equant phreatic bright to non-luminescent meteoric cement, laminar calcrete and tubular rhyzocretion structures. Samples MPUM13534, MPUM13535, and MPUM13539 (Port Bhéal an Dúin and Bungowla) are indicative of subtidal and higher energy settings with respect to the Burren area, as suggested by the grainstone to packstone texture, abundance of red algae *Ungdarella* associated with *Fasciella* and few *Koninckopora* and almost absent palaeoberesellids. Benthic foraminifers are common and confirm higher hydrodynamic conditions with the occurrence of eostaffellids and archaediscids. These facies were affected by subaerial exposure and meteoric diagenesis (skeletal grain micritization, vadose non-luminescent pendant and meniscus cement and phreatic equant sparite, root mat with alveolar texture due to palaeosol formation).

Sample MPUM13536 belongs to the Slievenaglasha Formation (Black Fort) and displays a different skeletal composition with common gastropods and bivalves and sparse red algae, suggesting a deeper environment of deposition, but still in the photic zone. There is no evidence of meteoric diagenesis, but intense micritisation forming grains with micrite envelopes, bright luminescent skeletal grains due to shallow burial recrystallisation, quenched dull luminescent drusy sparite replacing gastropod and bivalve shells and filling interparticle space during burial diagenesis.

4.2. Shell preservation: microstructure, petrographic, CL and geochemical analyses

SEM analysis indicates that the shell fabric is pristine (Figs. 8–9). The microstructure comprises a pseudopunctate laminar secondary and a thick columnar tertiary layer; the primary layer is absent due to dissolution. There are frequent intercalations of secondary and tertiary layers (Fig. 8A, D; Fig. 9D) both in the inner part of the posterior region and anteriorly, where the shell is thinner, and the contacts between fibers and columns are well-preserved. The columns of the tertiary layer are very clear and compact, and generally, there is no sign of calcite crystals with a rhombohedral morphology in the columnar layer, which argues against recrystallisation (Casella et al., 2018). There are major (annual) growth lines with a distinctive irregularly microgranular texture (Fig. 9A-B), and there are thin growth steps inside each column, 4–5 μm-thick, which in turn contain thin accretionary lines that may represent diurnal (light-mediated) growth banding (Fig. 9E-F).

Petrographic and cathodoluminescence investigations (Supplementary Table S4; Supplementary Figs. S3-S4) show that the shells analysed for geochemistry from Inishmore are largely non-luminescent, while those from the Burren are luminescent to a variable extent. Here, some shell portions are non-luminescent, while others show a blotchy bright luminescence – mostly in the laminar secondary layer, which was not sampled for isotope and trace element analyses. Fractures filled by non-luminescent to dull or bright luminescent to dull sparite cross the brachiopod shells.

The analysis of the microfacies associated with the analysed shells suggests burial diagenesis affecting the Burren limestones, while meteoric diagenesis and features related to palaeosol development affected the limestones of the Aillwee Member at Inishmore.

The full results of the elemental analysis are reported in the Supplementary Material (Supplementary Fig. S1; Supplementary Table S1-S2); here we summarise the most relevant results to our study, focusing on elements commonly used to diagnose diagenetic alteration (Mg, Mn, Fe, Sr) (Table 2). Specimens from Poulsallagh show Mg concentrations between 1255 and 5348 ppm (MPUM13528) and 1222 and 3423 ppm (MPUM13529). Mn is low and comparable between the two specimens, 1–46 ppm. Fe is higher (74–173 ppm) and Sr is lower (244–844 ppm) in MPUM13529 compared to MPUM13528 (Fe: 35–77 ppm, Sr: 215–1092 ppm). In the anterior part of the shell of specimen MPUM13528 (from sample #31), there is a decrease in Sr (<470 ppm) and an increase in Mn (>21 ppm) concentrations.

The specimen from Black Fort (MPUM13536) has Mg values between 2144 and 4662 ppm, low Mn (0.2–0.7 ppm) and Fe (56–64 ppm) and higher Sr (931–1434 ppm). Specimens from Port Bhéal an Dúin (MPUM13534–13535) show similar values of Mg, Mn, Fe and Sr (Table 2), with generally low Mn and Fe, and high Sr. Specimen from Port Mainistir (MPUM13532) has comparable values with the other Inishmore specimens.

Trace element values (Mg, Mn, Fe, Sr) observed in the analysed specimens fall within the range of variability reported in living brachiopods (e.g., Ullmann et al., 2017; Rollion-Bard et al., 2019; Crippa et al., 2025) and for well-preserved fossil congeneric species. The elemental concentrations show a heterogeneous distribution throughout the shell, reflecting the natural variations observed in fossil and living brachiopods (Cusack et al., 2008; Brand et al., 2011; Brand et al., 2025). Also, the tertiary layer of living brachiopods is generally depleted in TE (Rollion-Bard et al., 2019; Crippa et al., 2025), which may explain some of the low values recorded here. Concerning congeneric species, Angiolini et al. (2012) reported Sr > 700 ppm, Mg > 2500 ppm, Mn < 60 ppm, Fe < 300 ppm in *G. okensis* (Sarytcheva, 1928) from the UK. Armendáriz et al. (2008), in their study of *Gigantoproductus* sp.

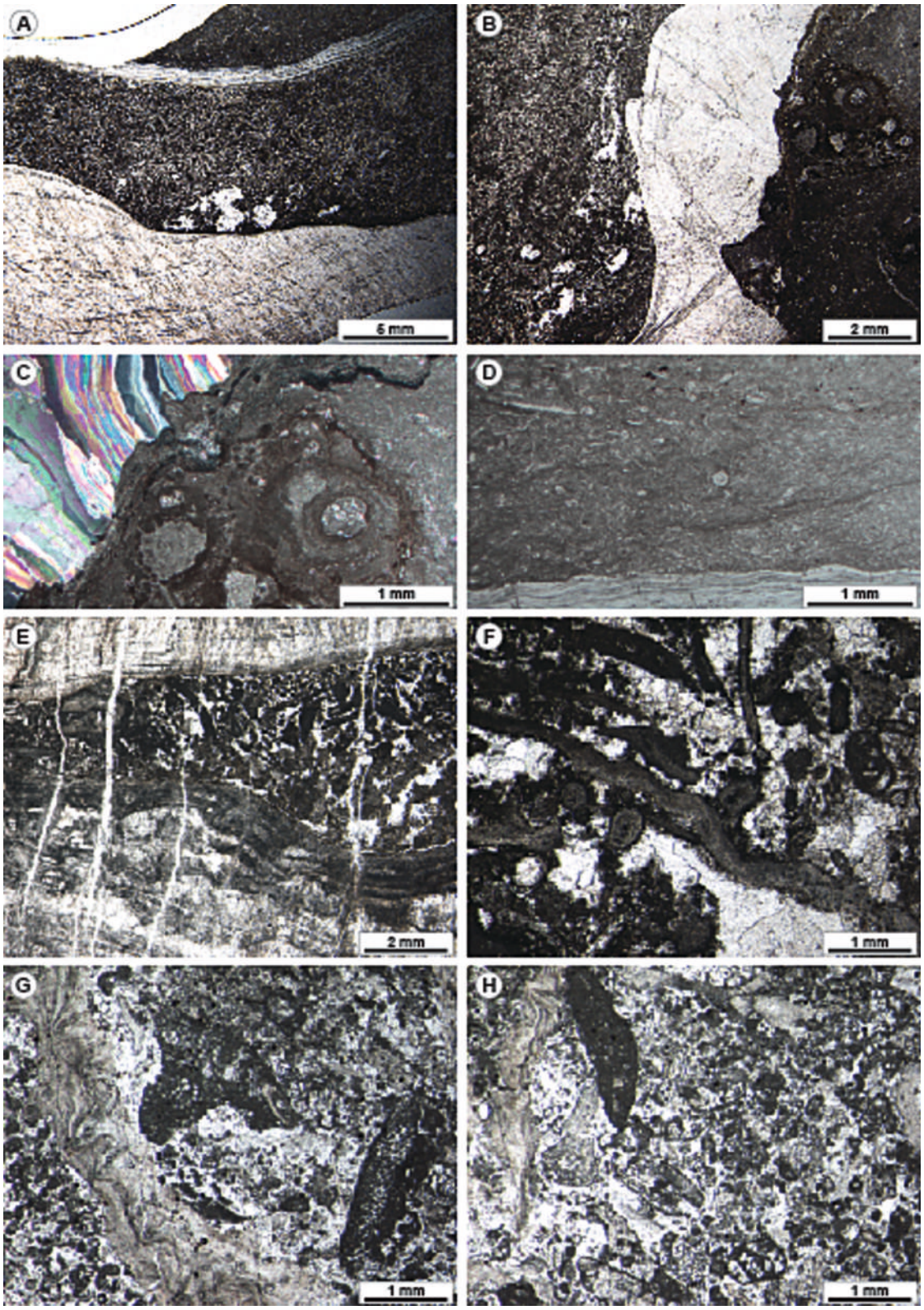

Fig. 6. Microfacies of the Burren Formation on Inishmore. A-B) Brachiopod shell infilled by skeletal peloidal packstone to wackestone affected by vuggy dissolution (left of shell) and development of laminar and tubular rhyzocretion (right of shell) due to subaerial exposure and palaeosol development (sample MPUM13532). C) Crossed polarised image showing on the left the brachiopod shell and on the right the tubular laminated rhyzocretion (sample MPUM13532). D) Palaeoberesellid algae wackestone (sample sample MPUM13532). E) Brachiopod shell infilled by peloidal grainstone to packstone with micritised skeletal grains and red algae *Ungdarella* and *Fasciella*, the whole texture is crossed by parallel fractures filled by burial sparite cement (sample MPUM13534). F) Detail of patches red algae *Ungdarella* boundstone strongly micritised and with meniscus cement due to subaerial exposure and meteoric diagenesis (sample MPUM13534). G) Peloidal skeletal grainstone to packstone with *Koninckopora*, *Ungdarella* and calcispheres (sample MPUM13535). H) Skeletal grainstone with red algae *Ungdarella* and *Fasciella* associated with *Omphalotis* foraminifer (sample MPUM13535). (For interpretation of the references to colour in this figure legend, the reader is referred to the web version of this article.)

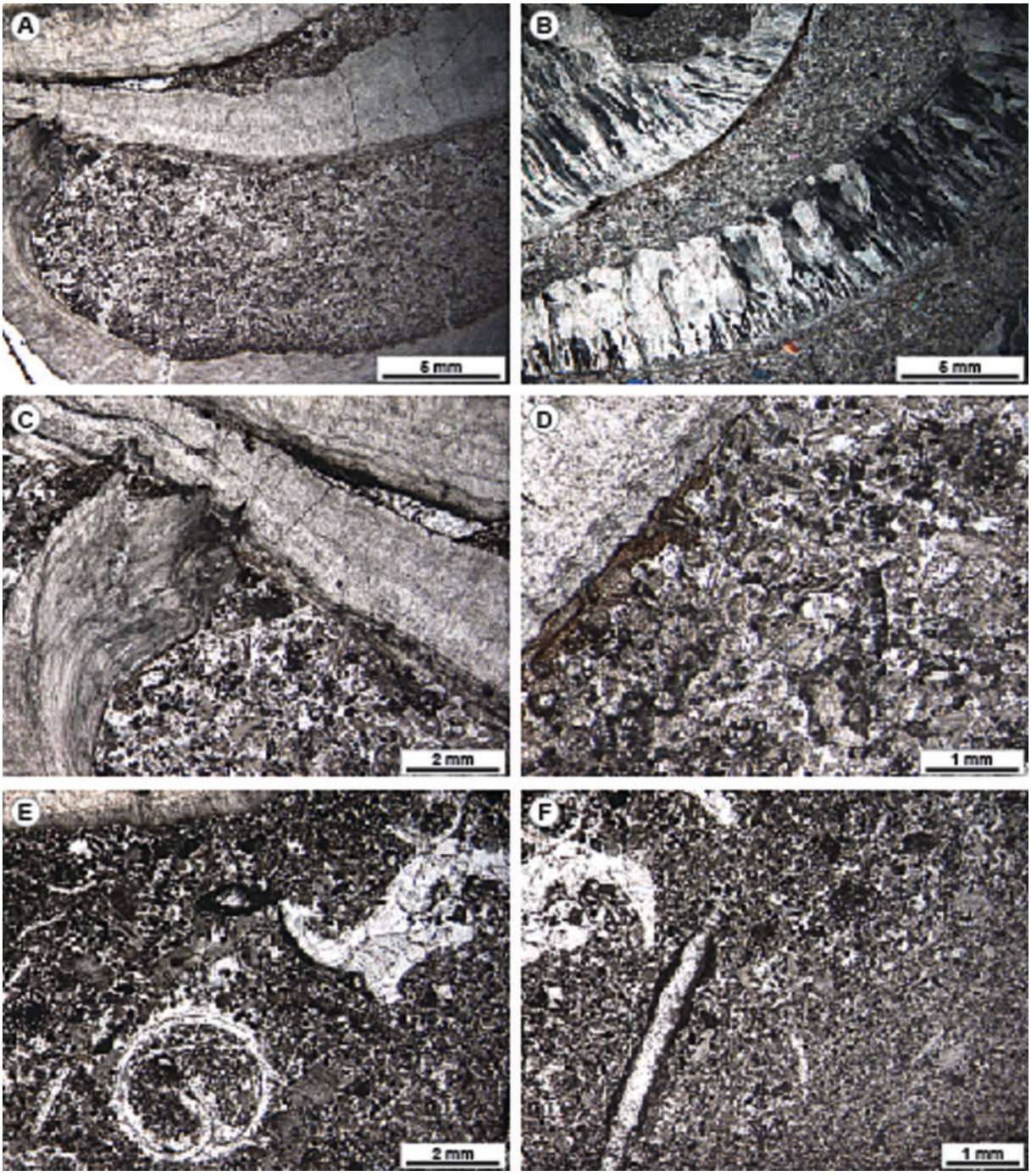

Fig. 7. Microfacies of the Burren Formation on Inishmore. A-B) Photomicrographs in parallel and crossed polarizers showing the brachiopod shells and the surrounding algal peloidal grainstone to packstone (sample MPUM13539). C) Brachiopod shells with sutured contact due to compaction and pressure solution; sediment infill is an algal grainstone/packstone with common red algae *Ungdarella* and minor *Fasciella*. The top geopetal cavity between the shells is filled by blocky cement and alveolar micrite irregular laminae resembling palaeosoil and root mat related alveolar fabric (sample MPUM13539). D) Skeletal grainstone/packstone with abundant red algae *Ungdarella* and one fragment of *Koninckopora*; on the left, pendant fibrous meteoric vadose cement hanging from the brachiopod shell (sample MPUM13539). E-F) Peloidal skeletal packstone with gastropods and micritised grains, coated grains with micrite envelops, echinoderm fragments and endothyrid foraminifers (sample MPUM13536). (For interpretation of the references to colour in this figure legend, the reader is referred to the web version of this article.)

specimens from Spain, considered samples with Mn values below 60 ppm and Fe values below 300 ppm as indicative of the best preserved material. However, Popp et al. (1986) and Mii et al. (2001) obtained higher values in Sr (1250–2500 ppm) and Mg (3000–6000 ppm) from Gigantoproductini brachiopods respectively from Belgium/UK and Russia. In general, for fossil brachiopods to be considered well preserved, a static approach - with cut-off values of Mn $<$ 250 ppm, and Sr $>$ 350 ppm - has been proposed (Popp et al., 1986; Bruckschen et al., 1999; Korte et al., 2003; Angiolini et al., 2012). However, such static limits are considered too inflexible and do not account for the natural variation of the ambient environment (Brand et al., 2011). In addition, Mn has been considered to be a more reliable indicator of diagenetic alteration than Sr (Popp et al., 1986; Bruckschen et al., 1999), and its concentration is low in the analysed specimens (along with that of Fe) excluding alteration.

Despite all elemental data falling within living and fossil brachiopod

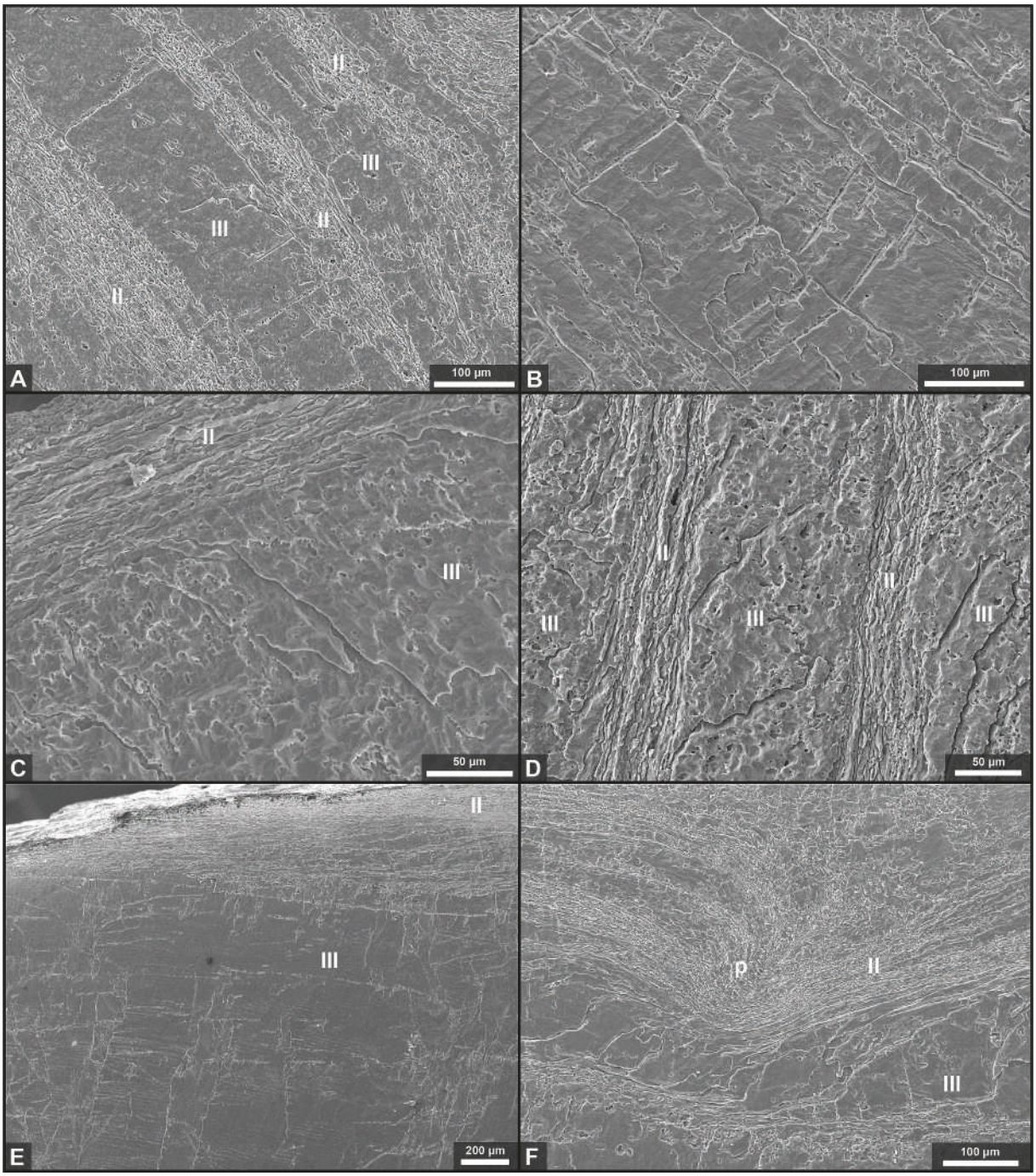

Fig. 8. SEM images showing the shell microstructure of *Gigantoproductus semiglobosus* (Part 1). A) MPUM13522, intercalations of laminar secondary layer (II) and columnar tertiary layer (III); B) MPUM13528, well-preserved columnar tertiary layer; C) MPUM13529, microstructural succession of the outermost part of the shell consisting of laminar secondary layer (II) with minor alteration in the form of laminae coalescence, and columnar tertiary layer (III); D) MPUM13530, intercalations of laminar secondary layer (II) and columnar tertiary layer (III); E) MPUM13532, microstructural succession of the shell consisting of laminar secondary layer (II) and columnar tertiary layer (III); F) MPUM13532, pseudopuncta (p) close to the transition between laminar secondary layer (II) and columnar tertiary layer (III).

ranges and their variability, indicating the generally good preservation of the shells, there are slight variations among the specimens. For instance, a decrease in Sr and an increase in Mn concentrations in the anterior part of MPUM13528, which also corresponds to a decrease in oxygen isotope values, but not in carbon, may indicate some diagenetic alteration in this part of the shell. MPUM13529 from the same locality, appears luminescent and has slightly higher Mn and Fe concentrations coupled with a slightly lower Sr concentration, compared to the other analysed specimens.

Based on a combination of SEM, CL and TE analyses, most of the analysed shells are considered well preserved, except for the anterior part of MPUM13528, and for MPUM13529, which, notwithstanding a preserved microstructure, appears locally luminescent and has different TE concentrations with respect to the other analysed shells, but still within the limits for well-preserved brachiopods. In fact, luminescence can also occur in living brachiopods (Barbin and Gaspard, 1995).

4.3. C and N isotopes from the shell organic fraction

The $\delta^{13}C_{org}$ and $\delta^{15}N_{org}$ were measured from organic fractions

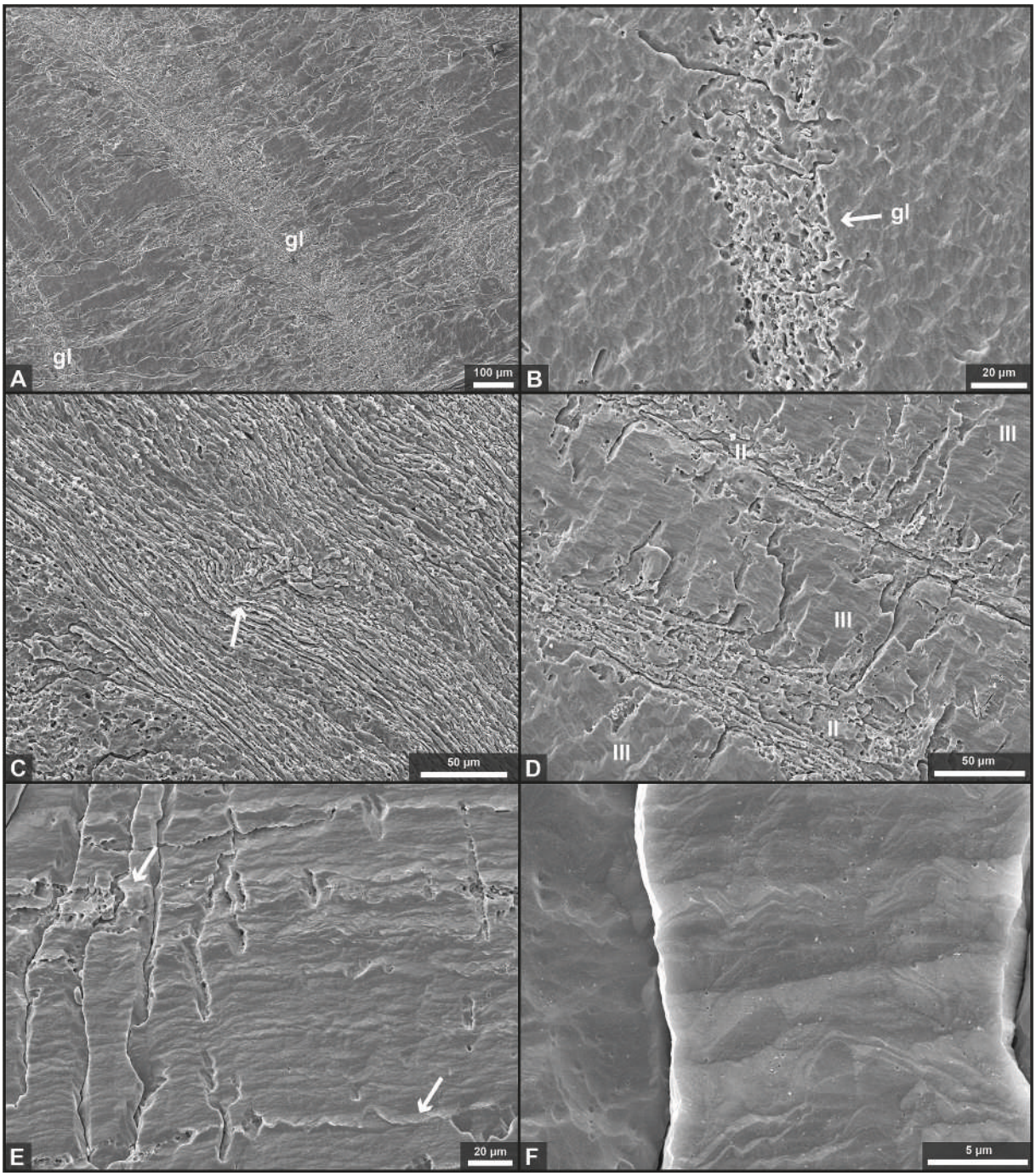

Fig. 9. SEM images showing the shell microstructure of *Gigantoproductus semiglobosus* (Part 2). A) MPUM13534, growth lines (gl) in the columnar tertiary layer; B) MPUM13535, details of a growth line (gl) in the columnar tertiary layer; C) MPUM13535, laminar secondary layer with pseudopuncta (white arrow); D) MPUM13536, intercalations of laminar secondary layer (II) and columnar tertiary layer (III); E) MPUM13536, growth steps inside the columns of the tertiary layer, some major growth lines are also visible (white arrows); F) MPUM13536, growth stages inside each column of the tertiary layer with thin accretionary lines which may represent diurnal growth banding.

isolated from the nanoscopic biocomposite, mesocrystal calcite of the columnar layer of three specimens of *G. semiglobosus* from two slightly different palaeoecological settings: a low to moderate energy shallow-water subtidal setting in the photic zone in the Aillwee Member at Poulsallagh, Burren (MPUM13528) and a moderate energy deeper subtidal setting in the Slievenaglasha Formation at the Black Fort, Inishmore (MPUM13537 and MPUM13538).

The $\delta^{13}C_{org}$ values of the shell organic matrix (SOM) are generally low and similar in both localities, ranging from −25.0 to −26.0 ‰, but the $\delta^{15}N_{org}$ values vary between −0.4 ‰ at Poulsallagh and + 7.1 ‰ at the Black Fort (Table 3).

Feng et al. (2018) investigated the carbon, nitrogen and sulphur isotopic signatures of the soft tissues and the shell organic matrix of mussel species with different symbionts and found that the SOM $\delta^{13}C_{org}$ values are typically higher with respect to the soft tissues by 4 ‰ and those of $\delta^{15}N_{org}$ by 1 ‰. Based on the study of Feng et al. (2018), the $\delta^{13}C_{org}$ and $\delta^{15}N_{org}$ values of the soft tissues of the investigated *G. semiglobosus* have been calculated from those of SOM and found to be −29.0 to −30.1 ‰ (VPDB) and − 1.4 ‰ and + 6.1 ‰ (Air), respectively (Table 3, Fig. 10).

Table 2
Summary of most relevant trace elements (Mg, Mn, Fe, Sr) from shell calcite. s is the sample standard deviation.

Specimen	Mg (ppm)	s	Mn (ppm)	s	Fe (ppm)	s	Sr (ppm)	s
MPUM13528								
Min	1255		1		35		215	
Max	5348		38		77		1092	
Mean	3015	1030	12	13	48	11	796	253
MPUM13529								
Min	1222		1		74		244	
Max	3423		46		173		844	
Mean	1868	437	14	9	107	28	489	115
MPUM13532								
Min	1279		0.1		32		879	
Max	4078		25		208		1774	
Mean	2453	656	1.4	4	61	43	1238	256
MPUM13534								
Min	1145		0.3		45		603	
Max	3561		26		149		1168	
Mean	2582	439	3	5	83	26	956	111
MPUM13535								
Min	1140		0.1		31		593	
Max	4993		9		194		1245	
Mean	2922	688	1.2	1.5	68	24	972	124
MPUM13536								
Min	2144		0.2		56		931	
Max	4662		0.7		64		1434	
Mean	3208	602	0.3	0.1	59	1.5	1155	100

Table 3
$\delta^{13}C_{org}$ and $\delta^{15}N_{org}$ values of the shell organic matrix (SOM) of the investigated *G. semiglobosus*. The isotope values of the soft tissues have been reconstructed from SOM following Feng et al. (2018). C and N (%) represent the values for the residue after dissolution of the shell.

Specimen	Sample ID	Museum n.	Location	$\delta^{13}C$ (‰) SOM	$\delta^{15}N$ (‰) SOM	N (%)	C (%)	C/N (mg/mg)	$\delta^{13}C$ (‰) soft tissue	$\delta^{15}N$ (‰) soft tissue
G. semiglobosus	BU2–3	MPUM13528	Poulsallagh	−25.3	−0.4	7.2	14.1	1.96	−29.3	−1.4
G. semiglobosus	AR11–9	MPUM13537	Black Fort	−25.0	+7.1	0.7	10	15.25	−29.0	+6.1
G. semiglobosus	AR11–10	MPUM13538	Black Fort	−26.1	+6.3	0.7	4.6	6.17	−30.1	+5.3

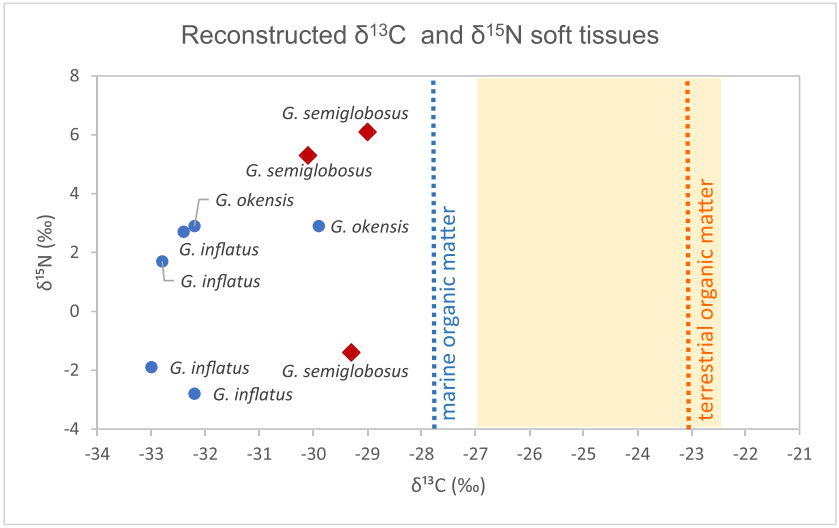

Fig. 10. A scatter plot of $\delta^{13}C_{org}$ and $\delta^{15}N_{org}$ showing the calculated isotope values of the soft tissues of the investigated specimens of *G. semiglobosus* (red diamonds) and other species from the same genus reported in Angiolini et al. (2019) (blue circles). The isotope values of the soft tissues have been reconstructed from shell organic matrix following Feng et al. (2018), also for the data of Angiolini et al. (2019) which were originally based on Mae et al. (2007). $\delta^{13}C_{org}$ values for Visean marine and terrestrial organic matter and the yellow rectangle representing theoretical values of $\delta^{13}C_{org}$ for the soft tissues of species pursuing a strict suspension feeding strategy are from Angiolini et al. (2019). (For interpretation of the references to colour in this figure legend, the reader is referred to the web version of this article.)

4.4. O and C sclerochemistry

The maximum, minimum and mean $\delta^{18}O$ and $\delta^{13}C$ values, as well as the mean of the differences between the maximum and minimum values in each growth increment recorded by each shell ($\Delta\delta^{18}O$, $\Delta\delta^{13}C$) and the corresponding temperatures calculated both with the Brand et al. (2019) equation and following the relation 1 ‰ ($\delta^{18}O$) = 4.3°C (Grossman and Ku, 1986) are summarised in Table 4.

Table 4
Summary of $\delta^{18}O$ and $\delta^{13}C$ values from shell calcite and calculated temperature variation.

Sample ID	Museum n.	Locality		$\delta^{18}O_{max}$ (‰)	$\delta^{18}O_{min}$ (‰)	$\delta^{18}O_{mean}$ (‰)	$\Delta\delta^{18}O$ (‰)	ΔT_1 (°C)	ΔT_2 (°C)	$\delta^{13}C_{max}$ (‰)	$\delta^{13}C_{min}$ (‰)	$\Delta\delta^{13}C$ (‰)	$\delta^{13}C_{mean}$ (‰)
BU2–10	MPUM13529	Burren	Poulsallagh	−4.0	−6.3	−5.4	1.2	7.0	5.2	+2.2	+1.2	0.5	+1.7
BU2–3	MPUM13528	Burren	Poulsallagh	−2.8	−6.9	−5.0	1.3	7.4	5.6	+2.6	−0.9	0.8	+1.5
AR11–5	MPUM13536	Inishmore, Aran Islands	Black Fort	−2.5	−5.1	−3.8	0.9	4.6	3.9	+3.8	−1.9	1.5	+0.6
AR10–28	MPUM13535	Inishmore, Aran Islands	Port Bhéal an Duin	−2.0	−4.7	−3.1	1.2	6.2	5.2	+1.9	−4.5	2.9	−0.5
AR10–16	MPUM13534	Inishmore, Aran Islands	Port Bhéal an Duin	−2.0	−6.1	−3.5	1.4	7.4	6.1	+1.1	−3.3	0.8	−0.6
AR2–5	MPUM13532	Inishmore, Aran Islands	Port Mainistir	−3.7	−7.1	−5.1	1.9	11.1	8.2	+2.5	−5.8	3.6	−1.7

Four samples in specimens MPUM13534, and one sample in MPUM13535 were excluded from the analysis, as they were located near fractures.

Growth lines, independently identified within the shell in peels and thin sections, correspond with the highest $\delta^{18}O$ values, thus with the lowest temperatures and define annual cycles. There are four to eight growth increments for each shell (Figs. 11–12). Cross plots of $\delta^{18}O$ vs $\delta^{13}C$ values are reported in Fig. 13.

Burren shells. The two shells from the Aillwee Member at Poulsallagh record similar $\Delta\delta^{18}O$ values, 1.3 ‰ in specimen MPUM13528 and 1.2 ‰ in specimen MPUM13529, respectively corresponding to a ΔT_1 of 7.4 °C and 7 °C, and a ΔT_2 of 5.6 °C and 5.2 °C. $\Delta\delta^{13}C$ values are similar in the two specimens (0.8 ‰ in MPUM13528 and 0.5 ‰ in MPUM13529), as well as their $\delta^{13}C_{mean}$ values (+1.5 ‰ and + 1.7 ‰, respectively), which represent the highest $\delta^{13}C_{mean}$ values recorded from the examined specimens.

Inishmore shells. Shells from the Aillwee Member at Port Bhéal an Dúin record similar $\Delta\delta^{18}O$ values, 1.4 ‰ in specimen MPUM13534 and 1.2 ‰ in specimen MPUM13535, respectively corresponding to a ΔT_1 of 7.4 °C and 6.2 °C, and a ΔT_2 of 6.1 °C and 5.2 °C. $\Delta\delta^{13}C$ values are different between the two specimens, 0.8 ‰ in MPUM13534 and 2.9 ‰ in MPUM13535. However, the $\delta^{13}C_{mean}$ values are similar, −0.6 ‰ and − 0.5 ‰.

The MPUM13532 shell from Port Mainistir records a $\Delta\delta^{18}O$ value of

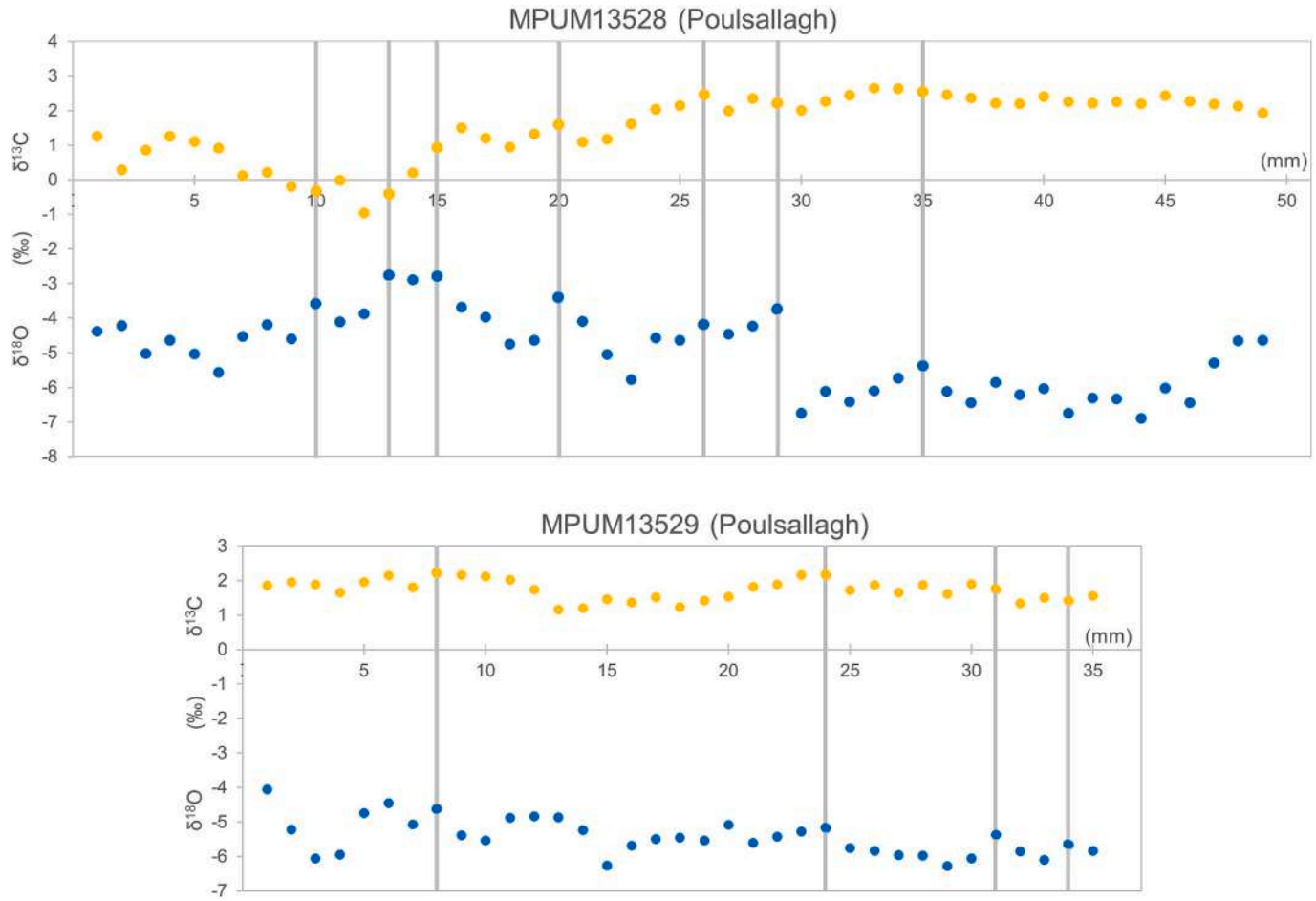

Fig. 11. $\delta^{18}O$ (blue circles) and $\delta^{13}C$ (yellow circles) isotope profiles for specimens of *Gigantoproductus semiglobosus* from Poulsallagh, Burren Region. Grey vertical lines represent the position of the growth lines. (For interpretation of the references to colour in this figure legend, the reader is referred to the web version of this article.)

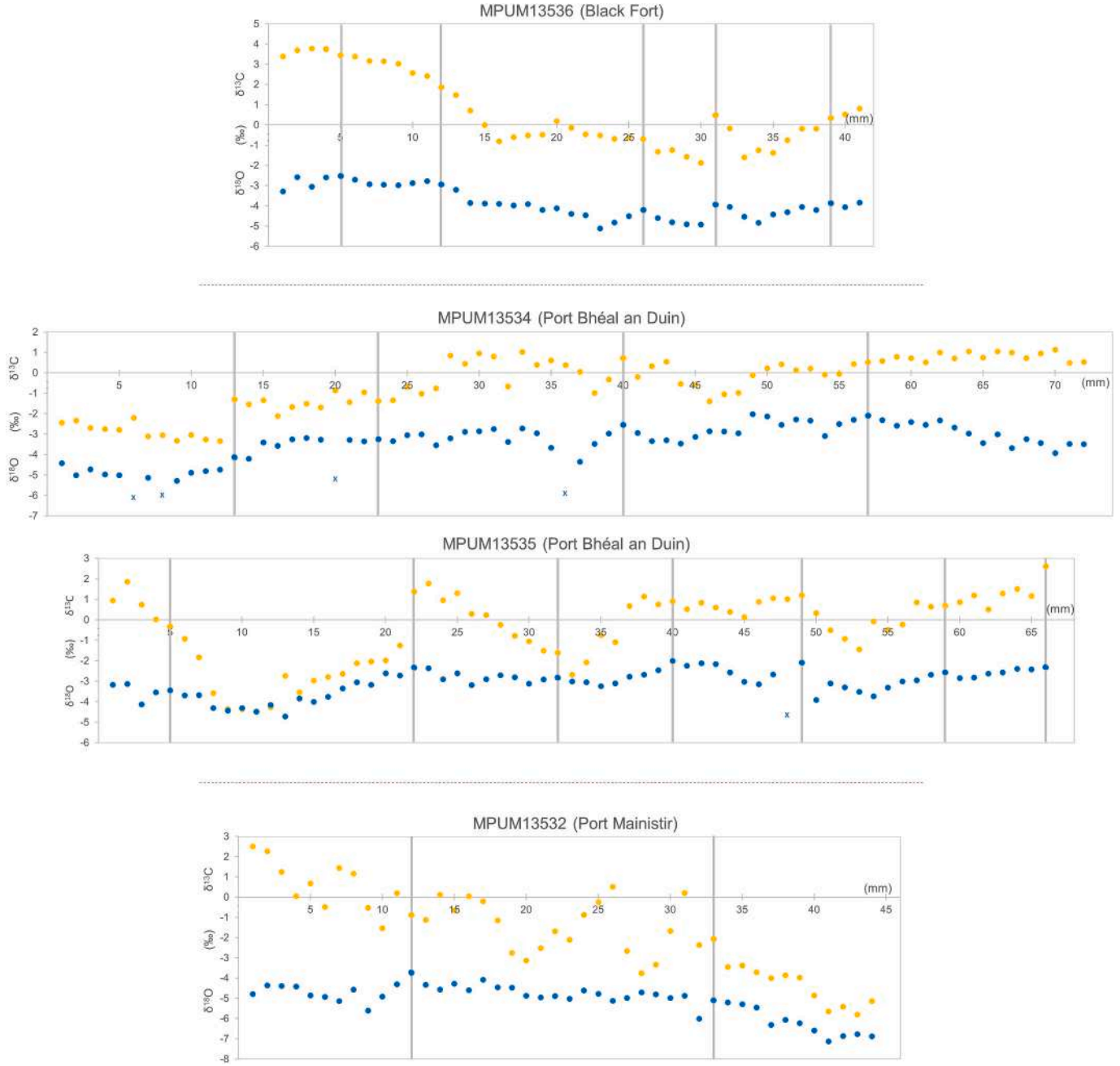

Fig. 12. $\delta^{18}O$ (blue circles) and $\delta^{13}C$ (yellow circles) isotope profiles for specimens of *Gigantoproductus semiglobosus* from Black Fort (AR11–5), Port Bhéal an Dúin (AR10–16, AR10–28) and Port Mainistir (AR2–5), Inishmore. Grey vertical lines represent the position of the growth lines. Blue crosses are outlier values not considered in the seasonal reconstruction. (For interpretation of the references to colour in this figure legend, the reader is referred to the web version of this article.)

1.9 ‰ corresponding to a ΔT_1 of 11.1 °C and a ΔT_2 of 8.2 °C, the highest value among the specimens here analysed. The $\Delta\delta^{13}C$ value is 3.6 ‰, whereas the $\delta^{13}C_{mean}$ value (−1.7 ‰) is the lowest among all the examined specimens. In this specimen, a very strong positive correlation between carbon and oxygen isotopic values has been observed (Fig. 13).

The MPUM13536 shell from the Slievenaglasha Formation at the Black Fort records a $\Delta\delta^{18}O$ value of 0.9 ‰ corresponding to a ΔT_1 of 4.6 °C and a ΔT_2 of 3.9 °C. The $\Delta\delta^{13}C$ value is 1.5 ‰, whereas the $\delta^{13}C_{mean}$ value is the highest among Inishmore specimens (+0.6 ‰). The mean of ΔT_1 and ΔT_2 in all the analysed shells is 6.5 °C.

The $\delta^{18}O$ and $\delta^{13}C$ values recorded from the available shells are in the range of values reported by Angiolini et al. (2012, 2019) for other species of *Gigantoproductus* from the UK, even if $\delta^{18}O$ values can be higher, and $\delta^{13}C$ values have a larger range of variation, both toward higher and lower values. The means of the $\delta^{18}O$ values of the Burren and Inishmore shells agree with those of microsampled Gigantoproductini from Russia (Mii et al., 2001), and from Belgium and the UK (Popp et al., 1986), but the mean $\delta^{13}C$ values tend to be lower.

5. Discussion

The present multidisciplinary analysis provides multiple lines of evidence across different spatial and biological scales. At the organismal scale, it contributes to elucidating the lifestyle and diet of *Gigantoproductus* species, as well as the factors that enabled them to achieve such exceptional sizes. From local to global scales, high-resolution stable-isotope analyses of their well-preserved shells allow for robust reconstructions of past climatic and environmental conditions, offering

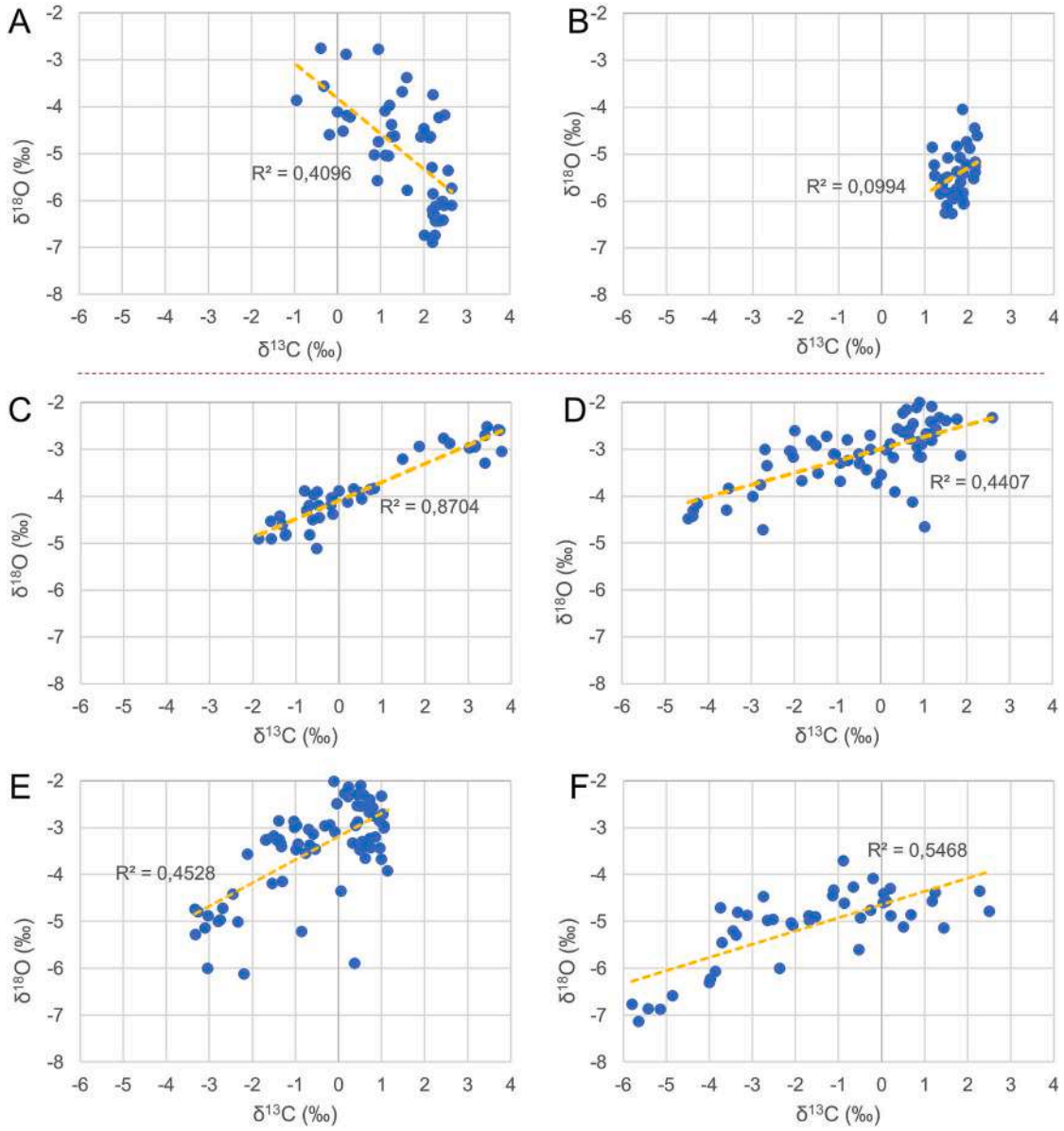

Fig. 13. Cross-plot diagrams of $\delta^{18}O$ and $\delta^{13}C$ with linear regression line and R^2 coefficient. A) Specimen MPUM13528, Poulsallagh, Burren; B) Specimen MPUM13529, Poulsallagh, Burren; C) Specimen MPUM13536, Black Fort, Inishmore; D) Specimen MPUM13535, Port Bhéal an Duin, Inishmore; E) Specimen MPUM13534, Port Bhéal an Duin, Inishmore; F) Specimen MPUM13532, Port Mainistir, Inishmore. The correlation is positive in except for A. It is statistically significant ($p < 0.05$), in all except for B.

new insights into the onset of the Late Palaeozoic Ice Age. The following sections discuss these aspects in detail.

5.1. *Lifestyle, diet, and gigantism*

Previous studies (e.g., Levin and Michener, 2002; O'Donnell et al., 2003; Mae et al., 2007; Dreier et al., 2012, 2014; Angiolini et al., 2019; Donnelly et al., 2024) indicated that the stable isotope compositions of carbon ($\delta^{13}C_{org}$) and nitrogen ($\delta^{15}N_{org}$) in the organic fractions included within shells are powerful proxies for identifying symbiotic relationships between marine organisms in the past. The SOM may be preserved because it is, to some extent, protected from diagenesis by the skeletal structure, which makes these proxies applicable to several types of fossil skeletons (O'Donnell et al., 2003; Muscatine et al., 2005; Mae et al., 2007; Dreier et al., 2012; Frankowiak et al., 2013; Tornabene et al., 2017; Angiolini et al., 2019; Killam et al., 2023), although Walton (1998) reported that 95 % of the amino acids from the intercrystalline proteins in brachiopods are in the free state after 120 kyr. However, that study did not quantify how much of the SOM could be lost, and its conclusion was not supported by later studies. In fact, Angiolini et al. (2019) had demonstrated that Mississippian species of *Gigantoproductus* from UK contain several aliphatic amino acids (alanine, leucine and serine).

The $\delta^{13}C_{org}$ and $\delta^{15}N_{org}$ SOM values mirror those of the soft tissues, typically differing by a few per mill (Mae et al., 2007; Feng et al., 2018), enabling the reconstruction of counterpart signatures of the soft tissues of fossil organisms. Vokhshoori et al. (2022) suggested that mean $\delta^{13}C_{org}$ and $\delta^{15}N_{org}$ values of bulk shell matrix protein in bivalves are always higher than those of the soft tissues, which facilitates the identification of the symbiotic relationships in marine organisms. A compilation of data from the literature on the biogeochemical signatures of the soft tissues of marine invertebrates with different trophic strategies is reported in Table 5. This compilation shows that the soft tissues of organisms with a non-symbiotic lifestyle are expected to have high

Table 5
Biogeochemical signatures of marine invertebrate soft tissues. The asterisk (*) indicates values of bulk organic shell matrix.

	$\delta^{13}C_{org}$	$\delta^{15}N_{org}$	References
Chemosymbiotic bivalves	−72‰ to −26‰	−20‰ to +7‰	Childress and Fisher, 1992; Mizota and Yamanaka, 2003; Cavanaugh et al., 2006; Mae et al., 2007; Dreier et al., 2014; Feng et al., 2018
Photosymbiotic bivalves*	−31.0 ‰ to −21 ‰	−2.5‰ to +4‰	Dreier et al., 2014; Killam et al., 2023
Filter-feeding bivalves	−24 ‰ to −17 ‰	+6 ‰ to +14‰	Rau and Hedges, 1979; Minagawa and Wada, 1984; Fry, 1988; Kwak and Zedler, 1997; Lorrain et al., 2002; Jennings and Warr, 2003; O'Donnell et al., 2003; Liénart et al., 2025
Symbiotic corals		+3 ‰ to +13 ‰	Tornabene et al., 2017; Donnelly et al., 2024
Non-symbiotic corals		+9‰ to +19 ‰	Tornabene et al., 2017; Donnelly et al., 2024
Mixotroph bivalves	−62 ‰ to −26 ‰	−16 ‰ to +5 ‰	Pile and Young, 1999; Dattagupta et al., 2004; Mckiness et al., 2005; Mae et al., 2007

$\delta^{13}C_{org}$/high $\delta^{15}N_{org}$, those with a photosymbiotic lifestyle to have low $\delta^{13}C_{org}$/intermediate $\delta^{15}N_{org}$, and the chemosymbiotic lifestyle to have low $\delta^{13}C_{org}$/low $\delta^{15}N_{org}$ (Table 5).

Recently, Donnelly et al. (2024) calculated the $\delta^{15}N_{org}$ offset between symbiotic and non-symbiotic corals and found it to be up to 4 ‰; the $\delta^{15}N_{org}$ values are generally lower in the symbiotic corals due to the efficient recycling of nitrogenous waste by symbionts, leading to minimal excretion of ^{14}N-rich ammonium into seawater. The carbon isotopic composition of tissues reflects that of the diet; for instance, methane in the case of organisms with methanotrophic endosymbionts and low-^{13}C carbon fixed by photosynthetic symbionts in photosymbiotic invertebrates. Heterotrophic feeding, consuming sources with higher $\delta^{13}C$ values (e.g., marine plankton, particulate organic matter), leads to a higher $\delta^{13}C$ in their tissues compared to organisms with symbionts (Feng et al., 2018), factoring in an increase of 1 ‰ relative to dietary carbon at each step-wise increase in the trophic level (O'Donnell et al., 2003).

Symbiotic metazoans are not exclusively dependent on nutrition derived from their symbionts. Indeed, some bivalves are mixotrophs, obtaining both carbon and nitrogen fixed by symbionts as well as nutrients acquired through filter feeding (Duplessis et al., 2004; Rossi et al., 2013). As a result, their soft tissues can exhibit variable isotopic signatures. Nevertheless, these organisms appear to rely more heavily on symbiont-derived compounds than on particulate feeding (Duperron et al., 2007; Dreier et al., 2014). Even within the same genus, species may display differences of several per mill in their $\delta^{13}C_{org}$ and $\delta^{15}N_{org}$ values, reflecting the balance between the symbiotic input and filter-feeding, which might also shift throughout the organism's ontogeny (Dreier et al., 2014; Schöne and Huang, 2021). Killam et al. (2023) observed a $\delta^{15}N_{org}$ shift from $> +4$ ‰ to −2.5 ‰ through ontogeny in giant clams, related to early heterotrophic feeding in juveniles, followed by mainly relying on photosynthetic symbionts at maturity.

The reconstructed $\delta^{13}C_{org}$ and $\delta^{15}N_{org}$ values of the soft tissues of *G. semiglobosus* are respectively low and intermediate (Table 3; Fig. 10), and their variation appears to fit with a mixotrophic lifestyle rather than with an exclusively filter-feeding strategy (Table 5). Compared with the data obtained by Angiolini et al. (2019) for the mixotrophs *Gigantoprodutus okensis* (Sarytcheva, 1928) and *Gigantoproductus inflatus* (Sarytcheva, 1928) from Derbyshire (Fig. 10), the $\delta^{13}C_{org}$ of the soft tissues of *G. semiglobosus* falls within their upper range. The $\delta^{15}N_{org}$ of the specimen from the Aillwee Member at Poulsallagh falls below the mean value of the species from the UK, but the $\delta^{15}N_{org}$ of the specimens from the Slievenaglasha Formation at the Black Fort is higher, possibly reflecting different food resources and different degrees of mixotrophy. For instance, a higher reliance on symbiont-fixed carbon is expected in a shallow well-lit marine environment, whereas a lower reliance is expected in environments with higher food supply.

Donnelly et al. (2024, their Fig. 5) have shown that an abundant food supply could lead to a wide range of increases in $\delta^{15}N_{org}$ values of symbiotic corals, whereas non-symbiotic corals have usually consistent values. Liénart et al. (2025) observed a lower $\delta^{15}N_{org}$ signature in bivalves from the oligotrophic Mediterranean Sea vs. bivalves of meso- to eutrophic Atlantic Ocean and English Channel; this is related to specific groups of phytoplankton using atmospheric nitrogen that is depleted in ^{15}N as their source when nutrients are lacking, which lowers the overall $\delta^{15}N$ of particulate organic matter transferred through the trophic chain.

The microfacies of the carbonate bed at the Black Fort locality indicates a subtidal moderate to low-energy setting – deeper than other localities because it lacks green algae and there are sparse ungdarellid red algae - which may have experienced a more consistent food supply, reflected in a higher $\delta^{15}N_{org}$. However, the abundance of green and red algae in the Aillwee Member at Poulsallagh suggests a well-lit environment, which might have enhanced symbiont-fixed carbon supply to the brachiopod host and thus higher $\delta^{15}N_{org}$ values. In contrast, no correlation was identified by Angiolini et al. (2019) between the two individual species, their respective palaeoenvironmental contexts, and the isotopic data, even if they also recorded a rather large variation in $\delta^{15}N_{org}$ values.

Intermediate $\delta^{15}N_{org}$ values coupled with low $\delta^{13}C_{org}$ seem to be more consistent with a photosymbiotic relationship rather than chemosymbiosis, as observed by Dreier et al. (2014). Also, all of the investigated specimens were living in the photic zone, as indicated by the microfacies analysis of the hosting rock. For the same reasons, Angiolini et al. (2019) favored the hypothesis that the species of *Gigantoproductus* from Derbyshire hosted photosymbionts, rather than chemosymbionts, even if these were from deeper middle ramp settings, quite different from the Burren and Inishmore ones. Angiolini et al. (2019) underlined that algal symbioses could have promoted the attainment of large and thick shells by the removal of CO_2. The occurrence of thin diurnal (light-mediated) accretionary lines in the columns of the shell of the species of *Gigantoproductus*, as those shown here (Fig. 9E-F), is in line with evidence for photosymbiosis in bivalves (Killam et al., 2023). This is further supported by the sulphur isotopic composition of sulphates in the shell of *Gigantoproductus* species from Russia provided by Kampschulte et al. (2001), which align with that of other brachiopod taxa (Kampschulte et al., 2001; Johnson et al., 2020) and exclude sulphur-based chemosymbiosis.

Angiolini et al. (2019) concluded that for two other species within the genus *Gigantoproductus*, the considerable size attained by *G. semiglobosus* may likewise be attributed to a mixotrophic strategy, whereby individuals derive energy and nutrients from both endosymbiotic microorganisms and suspended particulate organic matter acquired through filter feeding in different amounts, depending on the amount of food supply in the environment.

5.2. *Seasonality reconstruction from stable isotope profiles in shell calcite*

Several authors have used $\Delta\delta^{18}O$ values to reconstruct seasonal temperature variation from brachiopod fossil shells (Mii and Grossman, 1994; Angiolini et al., 2012; Roark et al., 2016; Garbelli et al., 2022; Viaretti et al., 2025).

Here, we show that at growth lines $\delta^{18}O$ values are at their maxima (Figs. 11–12) and temperatures at their minima, suggesting growth retardation (Crippa et al., 2025; Garbelli et al., 2025). Growth lines can thus be used to define annual growth increments in which to assess the temperature variation from $\Delta\delta^{18}O$ values, independently of assumptions about past seawater $\delta^{18}O$ values, and thus reducing diagenetic bias. Fujioka et al. (2025, their Fig. 4), investigating the effect of burial diagenesis on the microstructure and isotopic and chemical

compositions of living brachiopod shells through controlled artificial diagenesis experiments, observed a decrease in $\delta^{18}O$ values in altered shells, but seasonal variations were still preserved. Similar findings were reported by Angiolini et al. (2012) in fossil specimens of *G. okensis* from the Monsal Dale Limestone Formation of Derbyshire. These authors demonstrated that the annual periodicity seems to be retained as a residual signal within altered portions of the shell, suggesting that, while primary $\delta^{18}O$ values may be modified, the cyclic pattern can be preserved when diagenetic fluids locally permeated the shell. Although altered $\delta^{18}O$ values are systematically reduced by 4–6 ‰, they exhibit the same periodicity in both the preserved and altered regions of the shell.

In bivalve shells, Müller et al. (2017) and Moon et al. (2021), through thermally induced diagenesis experiments, observed that, despite the significant alteration of $\delta^{18}O$ values shifting toward lower values during the heating, the original seasonal temperature oscillations can be preserved. The diagenetic screening of *Gigantoproductus* shells shows that the shells of most of the available specimens are preserved. Only specimen MPUM13528 from Poulsallagh shows slightly higher concentrations of Mn (21–38 ppm) and lower Sr (215–470 ppm) in the anterior part, in correspondence with slightly lower $\delta^{18}O$ values, but there is no other sign of alteration, and the periodicity of the $\delta^{18}O$ signal is maintained as in the other parts of the shell. Additionally, the low content in Mn and Fe excludes significant alteration as a reason for the low Sr. The same holds for MPUM13529 from the same locality, which, besides having slightly lower Sr and slightly higher Fe concentrations, is luminescent and has lower $\delta^{18}O$ values, but it has the same periodicity of the $\delta^{18}O$ signal as the other specimens (Tables 2, 4; Fig. 11).

Most of the specimens show a moderate to strong positive correlation of $\delta^{18}O$ and $\delta^{13}C$ values (Fig. 13), which are interpreted as unrelated to diagenesis. In fact, a significative positive correlation of $\delta^{18}O$ and $\delta^{13}C$ has been observed in many living brachiopods taxa and ascribed to vital effects and to environmental controls (Takayanagi et al., 2015; Crippa et al., 2025; Garbelli et al., 2025). A regression analysis of the very large dataset published by Crippa et al. (2025) on living brachiopod species shows that the correlation between oxygen and carbon isotopes is very variable (from absent to strong), even in specimens of the same species or in specimens of different species but coexisting in the same environment.

Considering that $\Delta\delta^{18}O$ values in the brachiopod shells from the Aillwee Member at Poulsallagh and Port Bheal an Duin are 1.2 to 1.4 ‰ – but up to 1.9 ‰ in the shell from Port Mainistir, and 0.9 ‰ in the shell from the Slievenaglasha Formation at the Black Fort – the mean seasonal temperature variation recorded is 6.5 °C (mean of ΔT_1 and ΔT_2 in all the analysed shells) (Table 4). If this is comparable to that reported by Angiolini et al. (2012) from *G. okensis*, it is much higher with respect to records from low latitudes in similar settings at shallow water depths (from above to just below the normal wave base) both nowadays and in the distant past. For instance, living shells of *Tridacna gigas* (Linnæus, 1758) from the southern South China Sea record a $\Delta\delta^{18}O$ value of 0.4 ‰ that corresponds to a seasonal variation of less than 2 °C (Ma et al., 2020), in agreement with the annual seawater temperature variation set around 1.5–2 °C at low latitudes (Colin and Johnston, 2020). The same range of variation was reported by Roark et al. (2016) from Pennsylvanian brachiopods of central equatorial Pangea and by Garbelli et al. (2022) from uppermost Permian brachiopods of the Dolomites (Italy), near the palaeoequator at that time. However, at times of cold climate conditions, a high seasonal temperature variation has also been recorded at low palaeolatitudes (e.g., Viaretti et al., 2025), as discussed in the following paragraph. Indeed, a seasonal climate in northern Britain in the Asbian and Brigantian has been deduced from the study of tree rings in fossil wood (Falcon-Lang, 1999).

Comparing the ΔT of the different specimens here examined, the shell from Port Mainistir records the highest temperature variation (mean ΔT: 9.6 °C). This can be linked to the different palaeoenvironmental setting in which this specimen lived: a shallow water-lagoonal setting registering strong local influences and a higher variability of environmental parameters (temperature, freshwater input, seasonal riverine discharge, nutrient supply). In this case, the seasonal variations in temperature and in the isotopic composition of the water may have been amplified by freshening. This proximal setting could have been influenced by seasonal rainfall, as inferred from fossil tree rings (Falcon-Lang, 1999), leading to an increase in freshwater input, but without a significant change in salinity and in the $\delta^{18}O$ value of the seawater, as testified by the occurrence of marine organisms such as brachiopods and corals.

The $\delta^{13}C$ profiles show irregular variations, which may be in part related to vital effects (McConnaughey and Gillikin, 2008; von Allmen et al., 2010) or reflect the ambient environment. In the majority of specimens, the highest $\delta^{13}C$ values seem to correspond to the highest $\delta^{18}O$ values and are recorded in correspondence with the growth lines (Figs. 11, 12). This may indicate growth retardation in the colder and higher productivity season. The same has been observed in Lower Jurassic lithiotid bivalves from the lagoonal Rotzo Formation (northern Italy), where growth breaks coincide with the highest $\delta^{18}O$ and $\delta^{13}C$ values, at the cold and high productivity season (Posenato et al., 2022). This interpretation would be consistent with the growth strategy of the Gigantoproductini in relation to the geometry of their lophophore and their capacity to filter food resources. As already emphasized by Angiolini et al. (2019), given their simple lophophore, the growth of these species is favoured when food resources are scarce, possibly during the warm season. Thus, they may slow their rate of growth during the cold season.

The large $\Delta\delta^{13}C$ values recorded from the Aillwee Member at Port Bheal an Duin and Port Mainistir, coupled with lower $\delta^{13}C_{mean}$ values, may suggest changes in productivity, and thus high oscillations in food supply, during the growth of these shells (Table 4). The lowest $\delta^{13}C_{mean}$ value and highest $\Delta\delta^{13}C$ value are recorded in the shell from Port Mainistir, which lived in a lagoonal setting subjected to strong local influences, such as freshwater input, which would explain both the low $\delta^{13}C_{mean}$ values and the strong positive correlation between carbon and oxygen isotope values (e.g., Tao et al., 2013). Increased oxidation of the organic matter in the lagoon, and contamination with palaeosol-derived organic carbon, may have also caused an increased availability of ^{12}C to be incorporated into the shell calcite, and to a higher seasonal variation in productivity and freshwater input in this setting.

The $\Delta\delta^{13}C$ value is moderate in the specimen from the Slievenaglasha Formation at the Black Fort, while it is quite low in the Aillwee Member at Poulsallagh, where it is coupled with the highest $\delta^{13}C_{mean}$ values recorded in the available specimens (Table 4). This observation aligns with the interpretation of different degrees of mixotrophy proposed above, whereby the brachiopod from the Aillwee Member at Poulsallagh exhibits a greater dependence on symbiont-derived carbon, resulting in reduced annual $\delta^{13}C$ variability and, notably, elevated $\delta^{13}C_{mean}$ values. In scleractinian corals, for instance, under enhanced light availability, zooxanthellae do not preferentially assimilate [^{12}C] DIC during photosynthesis, but incorporate both [^{12}C]- and [^{13}C]DIC. Consequently, the internal carbon pool utilized by the coral is enriched in ^{13}C, as is the precipitated skeletal $CaCO_3$ (Reynaud-Vaganay et al., 2001). The specimens from the Slievenaglasha Formation could have relied on a higher food supply. There is evidence that chert-rich limestones became prominent in the succession (particularly in the middle part of Slievenaglasha Formation), suggesting a higher nutrient supply.

5.3. Implications for the LPIA

The Late Palaeozoic Ice Age (LPIA) commenced in the Late Devonian (Famennian) with a widespread glaciation (Streel et al., 2000; Caputo et al., 2008; Isaacson et al., 2008; Lakin et al., 2016; Caputo and Santos, 2020). This was followed by a more restricted glaciation in the Early Mississippian and then by the onset of sustained glaciation in the Middle Mississippian (late Visean) (Montañez, 2022). The LPIA continued until

the Early Permian (Sakmarian), with several phases and major climatic fluctuations in different palaeogeographic regions of Gondwana (Fielding et al., 2008; Isbell et al., 2012, 2021; Montañez, 2022; Griffis et al., 2023; Jurikova et al., 2025). Atmospheric CO_2 remained low throughout the LPIA, while its termination was driven by a rapid rise in atmospheric CO_2 around the Asselian-Sakmarian boundary (Jurikova et al., 2025).

The onset of sustained glaciation with the accumulation of more extensive continental ice thus began in the Middle Mississippian (late Visean). This is evidenced by glaciogenic deposits and glacially eroded surfaces in high-latitude Gondwanan regions (González, 1990; Caputo et al., 2008; Fielding et al., 2008; Gulbranson et al., 2010; Rosa et al., 2019; Caputo and dos Santos, 2020) and by the depth of incised valleys together with up to several tens of metres of high-frequency sea-level fluctuations at low palaeolatitudes in Euramerica (Soreghan and Giles, 1999; Smith and Read, 2000; Wright and Vanstone, 2001; Bishop et al., 2009; Barham et al., 2012; Ahern and Fielding, 2019, 2021; Fielding, 2021; Isbell et al., 2021; Montañez, 2022).

Among the far-field physical and chemical proxies used to interpret past glaciations (Isbell et al., 2021), isotopic signatures from marine fossil shells are particularly noteworthy for their potential to reconstruct past seasonality, that is, the variation of temperature that occurred at an instant in geologic time and its eventual evolution throughout a defined time interval (Crowley et al., 1986; Denton et al., 2005; Ferguson et al., 2011; Brocas et al., 2018).

Seasonality seems to have been a very important component in abrupt climate switches (Denton et al., 2005). An intensification of seasonality with constant mean temperatures has been associated with cool climatic phases and the occurrence of ice sheets at high latitudes in the Permian, Cretaceous, at the Eocene/Oligocene boundary and in the Pliocene-Pleistocene (Ivany et al., 2000; Pross and Klotz, 2002; Steuber et al., 2005; Eldrett et al., 2009; Ferguson et al., 2011; Hennissen et al., 2015; Crippa et al., 2016a; He et al., 2025; Mitra et al., 2025; Viaretti et al., 2025). In particular, Steuber et al. (2005) for the Cretaceous and Viaretti et al. (2025) for the Late Permian, observed an increased seasonality at low latitudes, corresponding to the onset of cold climate conditions. Recently, He et al. (2025), analyzing clumped isotopes of Lower Cretaceous (Valanginian) oyster shells from Madagascar, observed an increase in seasonality during the short-term cold interval, and lower amplitude seasonal variability in the warm interval. Mitra et al. (2025) conducted a multiproxy study on fossil oyster specimens from a palaeotropical Indian setting during the Middle Eocene Climatic Optimum; clumped-isotope thermometry of excellently-preserved shells suggests low seasonal temperature fluctuations (~3 °C) during this warm interval (early Bartonian), with seasonality increasing toward the cooler Oligocene. Thus, during different periods of geological time, low-palaeolatitude regions maintained low seasonal variability during warm intervals, whereas seasonality increased as the climate shifted toward colder conditions.

The unusually high temperature seasonality for low-palaeolatitude settings recorded in the examined *G. semiglobosus* shells from Ireland and by *G. okensis* from Derbyshire (Angiolini et al., 2012) - nearly three times greater than that recorded by uppermost Permian palaeoequatorial brachiopods (Garbelli et al., 2022) - is a far-field proxy for the onset of sustained glaciation in the late Asbian-Brigantian (late Visean); an additional evidence that this time interval was a major turning point in the dynamic glacial history of the LPIA. Additionally, reconstruction of palaeoseasonality can provide an additional proxy and may overcome some of the limits discussed by Isbell et al. (2021) – such as regional difference in evaporation, precipitation, freshwater influx, long-term temperature, salinity and circulation changes - in the use of $\delta^{18}O$ values obtained from marine benthic invertebrates to indicate times and intensity of glaciation/deglaciation.

An additional point deserves consideration. Qiao and Shen (2015) reported that species of *Gigantoproductus* were predominantly distributed in the circum-Palaeotethys region, occupying tropical to subtropical zones and inhabiting relatively shallow, warm-water shelf environments. Their flourishing during the late Visean suggests the persistence of warm climatic conditions at low latitudes during this interval. The low mean $\delta^{18}O$ values from the available shells, together with the results of Angiolini et al. (2012, 2019) and Popp et al. (1986) and Mii et al. (2001), consistently indicate warm tropical conditions.

The low-latitude Mississippian ocean waters did not experience significant cooling at the onset of the Gondwanan glaciation, a pattern that mirrors the situation during the final phase of the glaciation in the Asselian, when the tropical belt became narrower but did not experience a temperature decrease, only a reduction in its spatial extent (Angiolini et al., 2009). The same pattern, coupled with steepened latitudinal thermal gradients, was reported for the Cenozoic glacial tropics (Crame and Rosen, 2002) and for the Last Glacial Maximum (e.g., Ballantyne et al., 2005).

6. Limitation of the study

The sclerochemical analysis of carbon and oxygen isotope compositions of fossil brachiopod shells has the potential to record short-term variability in the ambient environment (e.g., Mii and Grossman, 1994; Grossman et al., 1996; Angiolini et al., 2012; Garbelli et al., 2022; Viaretti et al., 2025). However, fossil shells may be affected by diagenetic processes that can alter their isotopic composition; therefore, careful screening is required prior to geochemical analyses (e.g., Brand et al., 2011). A multiproxy approach can be applied, including examination of shell microstructure under SEM, cathodoluminescence (CL) observations, trace element (TE) analysis of shell calcite, and comparison of stable isotope compositions, as performed in this study.

This approach shows that most of the analysed shells can be considered well preserved. However, the petrographic analysis revealed localised alteration such as calcite-filled fractures and pressure solution features, which were mostly avoided during sampling. For instance, a few samples were excluded in specimens MPUM13534 and MPUM13535, as they were located near fractures. To minimise the inclusion of altered data that could bias interpretation, we used $\Delta\delta^{18}O$ values to reconstruct seasonality following two different approaches (Grossman and Ku, 1986 and Brand et al., 2019). Both our data and those of Angiolini et al. (2012) show that, although altered $\delta^{18}O$ values may be reduced by diagenesis, they record the same seasonal signal as the preserved regions of the shell or as preserved conspecific shells. This observation aligns with the results of Fujioka et al. (2025), suggesting that although diagenesis may alter absolute $\delta^{18}O$ values, it generally preserves their relative variability, thereby minimising the potential for interpretive bias.

In addition, using $\Delta\delta^{18}O$ values to reconstruct seasonal temperature variations may neglect changes in the isotopic composition of seawater related to freshwater input, particularly in the case of rainfall seasonality as documented at that time for northern Britain (Falcon-Lang, 1999). This potential bias can be assessed by analszing the depositional environment and the correlation between carbon and oxygen isotopes. Indeed, in one case, the higher amplitude of $\delta^{18}O$ variation recorded in the specimen from Port Mainistir has been attributed to the influence of freshwater. However, in most of the localities, the stenohaline faunas comprising corals, echinoids and crinoids besides brachiopods, exclude a change in salinity and thus in the $\delta^{18}O$ value of the seawater.

Overall, while some uncertainties related to preservation and environmental factors cannot be entirely ruled out, the applied screening procedures and analytical approach are expected to limit their impact on reconstructed seasonal patterns.

7. Conclusions

- Sclerochronological analyses of brachiopod shell calcite provide valuable insights into past seasonality, although those have been rarely conducted (Mii and Grossman, 1994; Grossman et al., 1996;

Angiolini et al., 2012; Garbelli et al., 2022; Viaretti et al., 2025). Isotopic signatures from the brachiopod shell organic matter stand out for their potential to reveal lifestyles and trophic strategies.

- The giant size attained by several species of *Gigantoproductus* is attributed to a mixotrophic strategy, whereby individuals derive energy and nutrients from both photosymbiotic microorganisms and suspended particulate organic matter acquired through filter feeding in varying amounts, depending on the availability of food supply in ambient environments.
- The high seasonality recorded by several species of *Gigantoproductus* from western Ireland and the UK at low palaeolatitudes supports the onset of a sustained glaciation in the late Visean.
- The palaeogeographic distribution of the species of *Gigantoproductus* and the geochemical composition of their shells indicate that low-latitude Mississippian ocean waters did not experience a temperature decrease at the onset of the Gondwanan glaciation.

Supplementary data to this article can be found online at https://doi.org/10.1016/j.palaeo.2025.113418.

CRediT authorship contribution statement

Lucia Angiolini: Writing – review & editing, Writing – original draft, Validation, Resources, Project administration, Methodology, Investigation, Funding acquisition, Formal analysis, Conceptualization. **Karem Azmy:** Writing – review & editing, Resources, Methodology, Formal analysis, Data curation. **Enrico Cannaò:** Writing – review & editing, Methodology, Formal analysis, Data curation. **Gaia Crippa:** Writing – review & editing, Resources, Methodology, Investigation, Formal analysis, Data curation. **Eamon Doyle:** Writing – review & editing, Resources, Methodology, Investigation. **Giovanna Della Porta:** Writing – review & editing, Methodology, Investigation, Formal analysis. **John Murray:** Writing – review & editing, Visualization, Methodology, Investigation. **Michael O'Connell:** Writing – review & editing, Investigation, Data curation. **Marco Viaretti:** Writing – review & editing, Methodology, Investigation, Formal analysis. **David A.T. Harper:** Writing – review & editing, Visualization, Investigation, Conceptualization.

Declaration of competing interest

The authors declare that they have no known competing financial interests or personal relationships that could have appeared to influence the work reported in this paper.

Acknowledgements

This work was supported by the European Union – Next Generation EU PRIN MUR 2022WEZR44 to Prof. C. Bottini. The work was also partly supported by the Italian Ministry for Universities and Research (MUR) through the project "Dipartimenti di Eccellenza 2023-27" (MV, GC, GDP, EC and LA). We thank Ethan Grossman and an anonymous reviewer for their insightful comments.

Data availability

The authors confirm that all data necessary for supporting the scientific findings of this paper have been provided.

References

Ahern, J.P., Fielding, C.R., 2019. Onset of the late Paleozoic glacioeustatic signal: a stratigraphic record from the paleotropical, oil shale-bearing Big Snowy Trough of Central Montana, USA. J. Sediment. Res. 89, 761–783. https://doi.org/10.2110/jsr.2019.44.

Ahern, J.P., Fielding, C.R., 2021. Carboniferous Manning Canyon Formation, northern Utah, USA: a carbonate-mud-dominated cyclothem motif recording the main onset of the late Paleozoic ice age. Sediment. Geol. 41, 105903. https://doi.org/10.1016/j.sedgeo.2021.105903.

Angiolini, L., Jadoul, F., Leng, M.J., Stephenson, M.H., Rushton, J., Chenery, S., Crippa, G., 2009. How cold were the early Permian glacial tropics? Testing Sea-surface temperature using the oxygen isotope composition of rigorously screened brachiopod shells. J. Geol. Soc. Lond. 166 (5), 933–945. https://doi.org/10.1144/0016-76492008-096R.

Angiolini, L., Stephenson, M., Leng, M.J., Jadoul, F., Millward, D., Aldridge, A., Andrews, J., Chenery, S., Williams, G., 2012. Heterogeneity, cyclicity and diagenesis in a Mississippian brachiopod shell of palaeoequatorial Britain. Terra Nova 24 (1), 16–26. https://doi.org/10.1111/j.1365-3121.2011.01032.x.

Angiolini, L., Crippa, G., Azmy, K., Capitani, G., Confalonieri, G., Della Porta, G., Griesshaber, E., Harper, D.A.T., Leng, M.J., Nolan, L., Orlandi, M., Posenato, R., Schmahl, W.W., Banks, V.J., Stephenson, M.H., 2019. The giants of the phylum Brachiopoda: a matter of diet? Palaeontology 62 (6), 889–917. https://doi.org/10.1111/pala.12433.

Aretz, M., Legrand-Blain, M., Vachard, D., Izart, A., 2019. Gigantoproductid and allied productid brachiopods from the "Calcaires a` Productus" (late Visean-Serpukhovian; Montagne Noire, southern France): taxonomy and palaeobiogeographical position in the Palaeotethys. Geobios 55, 17–40. https://doi.org/10.1016/j.geobios.2019.06.007.

Armendáriz, M., Rosales, I., Quesada, C., 2008. Oxygen isotope and Mg/ca composition of late Viséan (Mississippian) brachiopod shells from SW Iberia: Palaeoclimatic and palaeogeographic implications in northern Gondwana. Palaeogeogr. Palaeoclimatol. Palaeoecol. 268 (1–2), 65–79. https://doi.org/10.1016/j.palaeo.2008.07.008.

Ballantyne, A.P., Levine, M., Crowley, T.J., Liu, J., Baker, P.B., 2005. Meta-analysis of tropical surface temperatures during the Last Glacial Maximum. Geophys. Res. Lett. 32, L05712. https://doi.org/10.1029/2004GL021217.

Barbin, V., Gaspard, D., 1995. Cathodoluminescence of recent articulate brachiopod shells. Implications for growth stages and diagenesis evaluation. Geobios 28, 39–45. https://doi.org/10.1016/S0016-6995(95)80151-0.

Barham, M., Murray, J., Joachimski, M.M., Williams, D.M., 2012. The onset of the Permo-Carboniferous glaciation: reconciling global stratigraphic evidence with biogenic apatite δ18O records in the late Viséan. J. Geol. Soc. Lond. 169, 119–122. https://doi.org/10.1144/0016-76492011-102.

Barham, M., Murray, J., Sevastopulo, G.D., Williams, D.M., 2015. Conodonts of the genus *Lochriea* in Ireland and the recognition of the Viséan-Serpukhovian (Carboniferous) boundary. Lethaia 48, 151–171. https://doi.org/10.1111/let.12096.

Bishop, J.W., Montañez, I.P., Gulbranson, E.L., Brenckle, P.L., 2009. The onset of mid-Carboniferous glacio-eustasy: Sedimentologic and diagenetic constraints, Arrow Canyon, Nevada. Palaeogeogr. Palaeoclimatol. Palaeoecol. 276, 217–243. https://doi.org/10.1016/j.palaeo.2009.02.019.

Blakey, R.C., 2008. Gondwana paleogeography from assembly to breakup – A 500 m.y. odyssey. In: Fielding, C.R., Frank, T.D., Isbell, J.L. (Eds.), Resolving the Late Paleozoic Ice Age in Time and Space, 1–28. The Geological Society of America, Special Paper 441, Boulder.

Boer, W., Nordstad, S., Weber, M., Mertz-Kraus, R., Hönisch, B., Bijma, J., Raitzsch, M., Wilhelms-Dick, D., Foster, G.L., Goring-Harford, H., Nürnberg, D., Hauff, F., Kuhnert, H., Lugli, F., Spero, H., Rosner, M., van Gaever, P., de Nooijer, L.J., Reichart, G.J., 2022. New calcium carbonate nano-particulate pressed powder pellet (NFHS-2-NP) for LA-ICP-OES, LA-(MC)-ICP-MS and μXRF. Geostan. Geoanalytical Res. 46 (3), 411–432. https://doi.org/10.1111/ggr.12425.

Brand, U., Bitner, M.A., Logan, A., Azmy, K., Crippa, G., Angiolini, L., Colin, P., Grieshaber, E., Harper, E.M., Taddei Ruggiero, E., Haussermann, V., 2019. Brachiopod-based oxygen-isotope thermometer update and review. Riv. Ital. Palaeontol. Stratigr. 125 (3), 775–778. https://doi.org/10.13130/2039-4942/12228.

Brand, U., Rollion-Bard, C., Azmy, K., Bitner, M.A., Logan, A., Griesshaber, E., Simonet Roda, M., Schmahl, W., Gordillo, S., Asadi, N.V., Harper, E., Morrison, A.K., 2025. Li/Ca of modern brachiopods: a potential paleoseawater thermometer. Palaeogeogr. Palaeoclimatol. Palaeoecol. 669, 112928.

Brand, U., Logan, A., Bitner, M.A., Griesshaber, E., Azmy, K., Buhl, D., 2011. What is the ideal proxy of Palaeozoic seawater chemistry? Mem. Assoc. Australas. Palaeontol. 41, 9–24. https://doi.org/10.3316/informit.637671470793265.

Brocas, W.M., Felis, T., Gierz, P., Lohmann, G., Werner, M., Obert, J.C., Scholz, D., Kölling, M., Scheffers, S.R., 2018. Last interglacial hydroclimate seasonality reconstructed from tropical Atlantic corals. Paleoceanogr. Paleoclimatol. 33 (2), 198–213. https://doi.org/10.1002/2017PA003216.

Bruckschen, P., Oesmann, S., Veizer, J., 1999. Isotope stratigraphy of the European Carboniferous. Proxy signals for ocean chemistry, climate and tectonics. Chem. Geol. 161, 127–163.

Campbell, K.A., Bottjer, D.J., 1995. *Peregrinella*: an early cretaceous cold-seep-restricted brachiopod. Paleobiology 21, 461–478. https://doi.org/10.1017/S0094837300013488.

Caputo, M.V., dos Santos, R.O.B., 2020. Stratigraphy and ages of four early Silurian through late Devonian, early and Middle Mississippian glaciation events in the Parnaíba Basin and adjacent areas, NE Brazil. Earth Sci. Rev. 207, 103002. https://doi.org/10.1016/j.earscirev.2019.103002.

Caputo, M.V., Melo, J.H.G., Streel, M., Isbell, J.L., 2008. Late Devonian and early Carboniferous glacial records of South America. Geol. Soc. Am. Spec. Pap. 441, 161–173. https://doi.org/10.1130/2008.2441(11).

Casella, L.A., Griesshaber, E., Roda, M.S., Ziegler, A., Mavromatis, V., Henkel, D., Laudien, J., Häussermann, V., Neuser, R.D., Angiolini, L., Dietzel, M., Eisenhauer, A., Immenhauser, A., Brand, U., Schmahl, W.W., 2018. Micro-and nanostructures reflect the degree of diagenetic alteration in modern and fossil brachiopod shell calcite: a multi-analytical screening approach CL, FE-SEM, AFM, EBSD. Palaeogeogr.

Palaeocimatol. Palaeoecol. 502, 13–30. https://doi.org/10.1016/j.palaeo.2018.03.011.
Cavanaugh, C.M., Mckiness, Z.P., Newton, I.L.G., Stewart, F.J., 2006. Marine chemosynthetic symbioses. In: Dworkin, M., Falkow, S., Rosenberg, E., Stackebrandt, E. (Eds.), Prokaryotes. Volume 1: Symbiotic Associations, Biotechnology, Applied Microbiology. Springer, New York, N.Y, pp. 475–507.
Childress, J.J., Fisher, C.R., 1992. The biology of hydrothermal vent animals: physiology, biochemistry, and autotrophic symbioses. Oceanogr. Mar. Biol. 30, 337–441.
Colin, P.L., Johnston, T.S., 2020. Measuring temperature in coral reef environments: experience, lessons, and results from Palau. J Mar Sci Eng 8 (9), 680. https://doi.org/10.3390/jmse8090680.
Conil, R., Groessens, E., Laloux, M., Poty, E., Tournier, F., 1991. Carboniferous guide foraminifera, corals and conodonts in the Franco-Belgian and Campine Basins: their potential for widespread correlation. Cour. Forschungsinst. Senck. 130, 15–30.
Cowen, R., 1970. Analogies between the recent bivalve *Tridacna* and the fossil brachiopods Lyttoniacea and Richthofeniacea. Palaeogeogr. Palaeocimatol. Palaeoecol. 8, 329–344. https://doi.org/10.1016/0031-0182(70)90105-7.
Cowen, R., 1983. Algal symbiosis and its recognition in the fossil record. In: Tevesz, M.J. S., McCall, P.L. (Eds.), Biotic Interactions in Recent and Fossil Benthic Communities. Plenum, pp. 431–478. https://doi.org/10.1007/978-1-4757-0740-3_10.
Cózar, P., Somerville, I.D., 2021. Irish Serpukhovian revisited. Geol. J. 56 (3), 1403–1423. https://doi.org/10.1002/gj.3981.
Crame, J.A., Rosen, B.R., 2002. Cenozoic palaeogeography and the rise of modern biodiversity patterns. In: Crame, J.A., Owen, A.W. (Eds.), Palaeobiogeography and Biodiversity Change: The Ordovician and Mesozoic–Cenozoic Radiations, Geological Society, London, Special Publications, vol. 194, pp. 153–168. https://doi.org/10.1144/GSL.SP.2002.194.01.12.
Crippa, G., Angiolini, L., Bottini, C., Erba, E., Felletti, F., Frigerio, C., Hennissen, J.A.I., Leng, M.J., Petrizzo, M.R., Raffi, I., Raineri, G., Stephenson, M.H., 2016a. Seasonality fluctuations recorded in fossil bivalves during the early Pleistocene: Implications for climate change. Palaeogeogr. Palaeocimatol. Palaeoecol. 446, 234–251. https://doi.org/10.1016/j.palaeo.2016.01.029.
Crippa, G., Ye, F., Malinverno, C., Rizzi, A., 2016b. Which is the best method to prepare invertebrate shells for SEM analysis? Testing different techniques on recent and fossil brachiopods. Boll. Soc. Paleontol. Ital. 55 (2), 111–125. https://doi.org/10.4435/BSPI.2016.11.
Crippa, G., Jurikova, H., Leng, M.J., Zanchi, M., Harper, E.M., Rae, J.W.B., Savickaite, K., Viaretti, M., Angiolini, L., 2025. Brachiopods as archives of intrannual, annual, and interannual environmental variations. Limnol. Oceanogr. Lett. 10, 309–1402. https://doi.org/10.1002/lol2.70004.
Crowley, T.J., Short, D.A., Mengel, J.G., North, G.R., 1986. Role of seasonality in the evolution of climate during the last 100 million years. Science 231 (4738), 579–584. https://doi.org/10.1126/sci-ence.231.4738.579.
Cusack, M., Parkinson, D., Perez-Huerta, A., England, J., Curry, G.B., Fallick, A.E., 2008. Relationship between $\delta^{18}O$ and minor element composition of *Terebratalia transversa*. T. Roy. Soc. Edin-Earth 98, 439–445. https://doi.org/10.1017/S1755691008075671.
Dattagupta, S., Bergquist, D.C., Szalai, E.B., 2004. Tissue carbon, nitrogen, and sulfur stable isotope turnover in transplanted *Bathymodiolus childressi* mussels: relation to growth and physiological condition. Limnol. Oceanogr. 49 (4), 1144–1151. https://doi.org/10.4319/lo.2004.49.4.1144.
Denton, G.H., Alley, R.B., Comer, G.C., Broecker, W.S., 2005. The role of seasonality in abrupt climate change. Quat. Sci. Rev. 24 (10−11), 1159–1182. https://doi.org/10.1016/j.quas-cirev.2004.12.002.
Donnelly, H.A., Valadez-Ingersoll, M., Lin, M., Rivera, H.E., Tramonte, C.A., Davies, S. W., Wang, X.T., 2024. Ground truthing nitrogen isotopes as a symbiosis proxy using the facultatively symbiotic coral *Oculina arbuscula*. Front. Mar. Sci. 11, 1433382. https://doi.org/10.3389/fmars.2024.1433382.
Doyle, E., Orr, P., Murray, J., 2021. The earliest occurrence of the ichnogenus *Psilonichnus*: a new record from the Mississippian of the West of Ireland. Ichnos 28 (3), 208–216. https://doi.org/10.1080/10420940.2021.1932488.
Dreier, A., Stannek, L., Blumenberg, M., Taviani, M., Sigovini, M., Wrede, C., Thiel, V., Hoppert, M., 2012. The fingerprint of chemosymbiosis: origin and preservation of isotopic biosignatures in the nonseep bivalve *Loripes lacteus* compared with *Venerupis aurea*. FEMS Microbiol. Ecol. 81, 480–493. https://doi.org/10.1111/j.1574-6941.2012.01374.x.
Dreier, A., Loh, W., Blumenberg, M., Thiel, V., Hausereitner, D., Hoppert, M., 2014. The isotopic biosignatures of photo- vs. thiotrophic bivalves: are they preserved in fossil shells? Geobiology 12 (5), 406–423. https://doi.org/10.1111/gbi.12093.
Duperron, S., Fiala-Medioni, A., Caprais, J.C., Olu, K., Sibuet, M., 2007. Evidence for chemoautotrophic symbiosis in a Mediterranean cold seep clam (Bivalvia: Lucinidae): comparative sequence analysis of bacterial 16S rRNA, APS reductase and RubisCO genes. FEMS Microbiol. Ecol. 59, 64–70. https://doi.org/10.1111/j.1574-6941.2006.00194.x.
Duplessis, M.R., Dufour, S.C., Blankenship, L.E., Feldbeck, H., Yayanos, A.A., 2004. Anatomical and experimental evidence for particulate feeding in *Lucinoma aequizonata* and *Parvilucina tenuisculpta* (Bivalvia: Lucinidae) from the Santa Barbara Basin. Mar. Biol. 145, 551–561. https://doi.org/10.1007/s00227-004-1350-6.
Eldrett, J.S., Greenwood, D.R., Harding, I.C., Huber, M., 2009. Increased seasonality through the Eocene to Oligocene transition in northern high latitudes. Nature 459 (7249), 969–973. https://doi.org/10.1038/nature08069.
Falcon-Lang, H.J., 1999. The early Carboniferous (Courceyan-Arundian) monsoonal climate of the British Isles: evidence from growth rings in fossil woods. Geol. Mag. 136, 177–187.
Feng, D., Peckmann, J., Li, N., Kiel, S., Qiue, J.-W., Liang, Q., Carneyg, R.S., Pengh, Y., Taof, J., Chen, D., 2018. The stable isotope fingerprint of chemosymbiosis in the shell organic matrix of seep-dwelling bivalves. Chem. Geol. 479, 241–250. https://doi.org/10.1016/j.chemgeo.2018.01.015.
Ferguson, J.E., Henderson, G.M., Fa, D.A., Finlayson, J.C., Charnley, N.R., 2011. Increased seasonality in the Western Mediterranean during the last glacial from limpet shell geochemistry. Earth Planet. Sci. Lett. 308 (3–4), 325–333. https://doi.org/10.1016/j.epsl.2011.05.054.
Fielding, C.R., 2021. Late Palaeozoic cyclothems–a review of their stratigraphy and sedimentology. Earth Sci. Rev. 217, 103612. https://doi.org/10.1016/j.earscirev.2021.103612.
Fielding, C.R., Frank, T.D., Isbell, J.L., 2008. The late Paleozoic ice age — A review of current understanding and synthesis of global climate patterns. In: Fielding, C.R., Frank, T.D., Isbell, J.L. (Eds.), Resolving the Late Paleozoic Ice Age in Time and Space, Geol. Soc. Am. Spec. Pap, vol. 441, pp. 343–354. https://doi.org/10.1130/2008.2441(24).
Frankowiak, K., Mazur, M., Gothmann, A.M., Stolarski, J., 2013. Diagenetic alteration of Triassic coral from the aragonite Konservat-Lagerstatte in Alakir Cay, Turkey: implications for geochemical measurements. Palaios 28, 333–342. https://doi.org/10.2110/palo.2012.p12-116r.
Fry, B., 1988. Food web structure on Georges Bank from stable C, N, and S isotopic compositions. Limnol. Oceanogr. 33, 1182–1190. https://doi.org/10.4319/lo.1988.33.5.1182.
Fujioka, H., Suzuki, K., Takayanagi, H., Tasumi, E., Yamamoto, K., Ohfuji, H., Miyajima, T., Iryu, Y., 2025. Effects of artificial diagenetic alteration on the microstructure, isotopic composition, and metal element concentrations in brachiopod shells. Geochem. J. 59, 96–117. https://doi.org/10.2343/geochemj.GJ25005.
Gallagher, S.J., 1996. The stratigraphy and cyclicity of the late Dinantian platform carbonates in parts of southern and western Ireland. In: Strogen, P., Somerville, I.D., Jones, G.L. (Eds.), Recent Advances in Lower Carboniferous Geology. Geol. Soc. Spec. Publ., 107, pp. 239–251. https://doi.org/10.1144/GSL.SP.1996.107.01.17.
Gallagher, S.J., MacDermot, C.V., Somerville, I.D., Pracht, M., Sleeman, A.G., 2006. Biostratigraphy, microfacies and depositional environments of Upper Viséan limestones from the Burren region, County Clare, Ireland. Geol. J. 41, 61–91. https://doi.org/10.1002/gj.1033.
Garbelli, C., Angiolini, L., Posenato, R., Harper, E.M., Lamare, M.D., Shi, G.R., Shen, S.Z., 2022. Isotopic time-series ($\delta^{13}C$ and $\delta^{18}O$) obtained from the columnar layer of Permian brachiopod shells are a reliable archive of seasonal variations. Palaeogeogr. Palaeocimatol. Palaeoecol. 607, 111264. https://doi.org/10.1016/j.palaeo.2022.111264.
Garbelli, C., Lamare, M.D., Harper, E.M., 2025. Brachiopod shells as archives of seasonality: insights from growth lines, microstructure, $\delta^{13}C$ and $\delta^{18}O$ values in *Calloria inconspicua*. Mar. Biol. 172 (7), 117. https://doi.org/10.1007/s00227-025-04675-8.
González, C.R., 1990. Development of the late Paleozoic glaciations of the South American Gondwana in western Argentina. Palaeogeogr. Palaeocimatol. Palaeoecol. 79, 275–287. https://doi.org/10.1016/0031-0182(90)90022-Y.
Griffin, W.L., Powell, W.J., Pearson, N.J., O'Reilly, S.Y., 2008. GLITTER: Data Reduction Software for Laser Ablation ICP-MS. Laser Ablation-ICP-MS in Earth Sciences. In: Sylvester, P. (Ed.), Laser Ablation ICP-MS in the Earth Sciences: Current Practices and Outstanding Issues, 40. Mineralogical Association of Canada. https://doi.org/10.3749/9780921294801.app02.
Griffis, N., Mundil, R., Montanez, I., Le Heron, D., Dietrich, P., Iannuzzi, R., 2023. A Carboniferous apex for the late Paleozoic icehouse. In: Lucas, S.G., DiMichele, W. A., Opluštil, S., Wang, X. (Eds.), Ice Ages, Climate Dynamics and Biotic Events: The Late Pennsylvanian World. Geol. Soc. Spec. Publ., vol. 535, pp. 117–129. https://doi.org/10.1144/SP535-2022-256.
Grossman, E.L., Ku, T.L., 1986. Oxygen and carbon isotope fractionation in biogenic aragonite: temperature effects. Chem. Geol. Isot. Geosci. Sect. 59, 59–74. https://doi.org/10.1016/0168-9622(86)90057-6.
Grossman, E.L., Mii, H.S., Zhang, C., Yancey, T.E., 1996. Chemical variation in Pennsylvanian brachiopod shells – diagenetic, taxonomic, microstructural, and seasonal effects. J. Sediment. Res. 66, 1011–1022.
Grossman, E.L., Yancey, T.E., Jones, T.E., Bruckschen, P., Chuvashov, B., Mazullo, S.J., Mii, H.S., 2008. Glaciation, aridification, and carbon sequestration in the Permo-Carboniferous. The isotopic record from low latitudes. Palaeogeogr. Palaeocimatol. Palaeoecol. 268, 222–233. https://doi.org/10.1016/j.palaeo.2008.03.053.
Gulbranson, E.L., Montanez, I.P., Schmitz, M.D., Limarino, C.O., Isbell, J.L., Marenssi, S. A., Crowley, J.L., 2010. High-precision U–Pb calibration of Carboniferous glaciation and climate history, Paganzo Group, NW Argentina. Geol. Soc. Am. Bull. 122, 1480–1498. https://doi.org/10.1130/b30025.1.
He, S., Wang, T., Spicer, R.A., Farnsworth, A., Mulch, A., Widdowson, M., Zhang, Q., Cai, F., Valdes, P.J., Wang, C., Randrianaly, H.N., Xie, J., Ding, L., 2025. Back to an ice-free future: early cretaceous seasonal cycles of sea surface temperature and glacier ice. Sci. Adv. 11, 18, eadr9417. https://doi.org/10.1126/sciadv.adr9417.
Hennissen, J.A., Head, M.J., De Schepper, S., Groeneveld, J., 2015. Increased seasonality during the intensification of Northern Hemisphere glaciation at the Pliocene–Pleistocene boundary~ 2.6 Ma. Quat. Sci. Rev. 129, 321–332. https://doi.org/10.1016/j.quascirev.2015.10.010.
Isaacson, P.E., Díaz-Martínez, E., Grader, G.W., Kalvoda, J., Bábek, O., Devuyst, F.X., 2008. Late Devonian–earliest Mississippian glaciation in Gondwanaland and its biogeographic consequences. Palaeogeogr. Palaeocimatol. Palaeoecol. 268 (3–4), 126–142. https://doi.org/10.1016/j.palaeo.2008.03.047.
Isbell, J.L., Henry, L.C., Gulbranson, E.L., Limarino, C.O., Fraiser, M.L., Koch, Z.J., Ciccioli, P.L., Dineen, A.A., 2012. Glacial paradoxes during the late Paleozoic ice age: evaluating the equilibrium line altitude as a control on glaciation. Gondwana Res. 22 (1), 1–19. https://doi.org/10.1016/j.gr.2011.11.005.

Isbell, J.L., Vesely, F.F., Rosa, E.L., Pauls, K.N., Fedorchuk, N.D., Ives, L.R., McNall, N.B., Litwin, S.A., Borucki, M.K., Malone, J.E., Kusick, A.R., 2021. Evaluation of physical and chemical proxies used to interpret past glaciations with a focus on the late Paleozoic Ice Age. Earth Sci. Rev. 221, 103756. https://doi.org/10.1016/j.earscirev.2021.103756.

Ivany, L.C., Patterson, W.P., Lohmann, K.C., 2000. Cooler winters as a possible cause of mass extinctions at the Eocene/Oligocene boundary. Nature 407 (6806), 887–890. https://doi.org/10.1038/35038044.

Jennings, S., Warr, K.J., 2003. Environmental correlates of large-scale spatial variation in the $\delta^{15}N$ of marine animals. Mar. Biol. 142, 1131–1140. https://doi.org/10.1007/s00227-003-1020-0.

Jochum, K.P., Weis, U., Stoll, B., Kuzmin, D., Yang, Q., Raczek, I., Jacob, D.E., Stracke, A., Birbaum, K., Frick, D.A., Günther, D., Enzweiler, J., 2011. Determination of reference values for NIST SRM 610–617 glasses following ISO guidelines. Geostand. Geoanal. Res. 35 (4), 397–429. https://doi.org/10.1111/j.1751-908X.2011.00120.x.

Jochum, K.P., Garbe-Schönberg, D., Veter, M., Stoll, B., Weis, U., Weber, M., Lugli, F., Jentzen, A., Schiebel, R., Wassenburg, J.A., Jacob, D.E., Haug, G.H., 2019. Nano-powdered calcium carbonate reference materials: significant progress for microanalysis? Geostand. Geoanal. Res. 43 (4), 595–609. https://doi.org/10.1111/ggr.12292.

Johnson, D.L., Grossman, E.L., Webb, S.M., Adkins, J.F., 2020. Brachiopod $\delta^{34}S_{CAS}$ microanalyses indicate a dynamic, climate-influenced Permo-Carboniferous sulfur cycle. Earth Planet. Sci. Lett. 546, 116428.

Jurikova, H., Garbelli, C., Whiteford, R., Reeves, T., Laker, G., Liebetrau, V., Gutjahr, M., Eisenhauer, A., Savickaite, K., Leng, M.J., Iurino, D.A., Viaretti, M., Tomašových, A., Zhang, Y., Wang, W., Shi, G.R., Shen, S.Z., Rae, J.W.B., Angiolini, L., 2025. Rapid rise in atmospheric CO2 ended the Late Palaeozoic Ice Age. Nat. Geosci. https://doi.org/10.1038/s41561-024-01610-2.

Kampschulte, A., Bruckschen, P., Strauss, H., 2001. The Sulphur isotopic composition of trace sulphates in Carboniferous brachiopods: implications for coeval seawater, correlation with other geochemical cycles and isotope stratigraphy. Chem. Geol. 175, 149–173.

Key Jr., M.M., Wyse Jackson, P.N., Hakansson, E., Patterson, W.P., Moore, M.D., 2005. Gigantism in Permian trepostomes from Greenland: Testing the algal symbiosis hypothesis using $d^{13}C$ and $d^{18}O$ values. 141–151. In: Moyano, H.I., Cancino, J.M., Wyse Jackson, P.N. (Eds.), Bryozoan Studies: Proceedings of the 13th International Bryozoology Association Conference, Concepción/Chile, 11–16 January 2004. CRC Press.

Kiel, S., Glodny, J., Birgel, D., Bulot, L.G., Campbell, K.A., Gaillard, C., Graziano, R., Kaim, A., Lazar, I., Sandy, M.R., Peckmann, J., 2014. The Paleoecology, Habitats, and Stratigraphic Range of the Enigmatic Cretaceous Brachiopod *Peregrinella*. PLoS One 9 (10), 1–19. https://doi.org/10.1371/journal.pone.0109260.

Killam, D., Das, S., Martindale, R.C., Gray, K.E., Paytan, A., Junium, C.K., 2023. Photosymbiosis and nutrient utilization in giant clams revealed by nitrogen isotope sclerochronology. Geochim. Cosmochim. Acta 359, 165–175. https://doi.org/10.1016/j.gca.2023.08.018.

Korte, C., Kozur, H.W., Bruckschen, P., Veizer, J., 2003. Strontium isotope evolution of late Permian and Triassic seawater. Geochim. Cosmochim. Acta 67, 47–62.

Kwak, T.J., Zedler, J.B., 1997. Food web analysis of southern California coastal wetlands using multiple stable isotopes. Oecologia 110 (2), 262–277. https://doi.org/10.1007/s004420050159.

Lakin, J.A., Marshall, J.E.A., Troth, I., Harding, I.C., 2016. Greenhouse to icehouse: a biostratigraphic review of latest Devonian–Mississippian glaciations and their global effects. In: Becker, R.T., Königshof, P., Brett, C.E. (Eds.), Devonian Climate, Sea Level and Evolutionary Events. Geol. Soc. Lon. Spec. Publ., 423(1), pp. 439–464. https://doi.org/10.1144/SP423.12.

Levin, L.A., Michener, R.H., 2002. Isotopic evidence for chemosynthesis-based nutrition of macrobenthos: the lightness of being at Pacific methane seeps. Limnol. Oceanogr. 47 (5), 1336–1345. https://doi.org/10.4319/lo.2002.47.5.1336.

Liénart, C., Fournioux, A., Garbaras, A., Blanchet, H., Briant, N., Dubois, S.F., Gangnery, A., Grouhel Pellouin, A., Le Monier, P., Lheureux, A., de Montaudouin, X., Savoye, N., 2025. Bivalve monitoring over French coasts: multi-decadal records of carbon and nitrogen elemental and isotopic ratios as ecological indicators of global change. Earth Syst. Sci. Data 17, 799–815. https://doi.org/10.5194/essd-17-799.

Lorrain, A., Paulet, Y.-M., Chauvaud, L., Savoye, N., Donval, A., Saout, C., 2002. Differential $\delta^{13}C$ and $\delta^{15}N$ signatures among scallop tissues: implications for ecology and physiology. J. Exp. Mar. Biol. Ecol. 275, 47–61. https://doi.org/10.1016/S0022-0981(02)00220-4.

Ma, X., Yan, H., Fei, H., Liu, C., Shi, G., Huang, E., Wang, Y., Qu, X., Lian, E., Dang, H., 2020. A high-resolution $\delta^{18}O$ record of modern Tridacna gigas bivalve and its paleoenvironmental implications. Palaeogeogr. Palaeoclimatol. Palaeoecol. 554, 109800. https://doi.org/10.1016/j.palaeo.2020.109800.

Mae, A., Yamanaka, T., Shimoyama, S., 2007. Stable isotope evidence for identification of chemosynthesis-based fossil bivalves associated with cold-seepages. Palaeogeogr. Palaeoclimatol. Palaeoecol. 245, 411–420. https://doi.org/10.1016/j.palaeo.2006.09.003.

McConnaughey, T.A., Gillikin, D.P., 2008. Carbon isotopes in mollusk shell carbonates. Geo-Mar. Lett. 28, 287–299. https://doi.org/10.1007/s00367-008-0116-4.

Mckiness, Z.P., Mcmullin, E.R., Fisher, C.R., Cavanaugh, C.M., 2005. A new bathymodioline mussel symbiosis at the Juan de Fuca hydrothermal vents. Mar. Biol. 148, 109–116. https://doi.org/10.1007/s00227-005-0065-7.

M'Coy, F., 1862. A Synopsis of the Characters of the Carboniferous Limestone Fossils of Ireland. Williams and Northgate, London, p. 207.

Mii, H.S., Grossman, E.L., 1994. Late Pennsylvanian seasonality reflected in the ^{18}O and elemental composition of a brachiopod shell. Geology 22 (7), 661–664. https://doi.org/10.1130/0091-7613(1994)022%3C0661:LPSRIT%3E2.3.CO;2.

Mii, H.S., Grossman, E.L., Yancey, T.E., Chuvashov, B., Egorov, A., 2001. Isotopic records of brachiopod shells from the Russian Platform—evidence for the onset of Mid-Carboniferous glaciation. Chem. Geol. 175, 133–147.

Minagawa, M., Wada, E., 1984. Stepwise enrichment of ^{15}N along food chains: further evidence and the relation between $\delta^{15}N$ and animal age. Geochim. Cosmochim. Acta 48, 1135–1140. https://doi.org/10.1016/0016-7037(84)90204-7.

Mitra, A., de Winter, N.J., Miloikovitch, T., Halder, K., Ledésert, B.A., Claeys, P., Müller, I.A., 2025. Habitat specific growth rate adaptation in oysters during early Bartonian: Effects of high temperature and low seasonality in the Indian palaeotropics. Paleoceanogr. Paleoclimatol. 40, e2025PA005129. https://doi.org/10.1029/2025PA005129.

Mizota, C., Yamanaka, T., 2003. Strategic adaptation of a deep-sea, chemosynthesis-based animal community: an evaluation based on soft body part carbon, nitrogen, and sulfur isotopic signatures. J. Jap. Benthol. 58, 56–69 (in Japanese with English abstract).

Montañez, I.P., 2022. Current synthesis of the penultimate icehouse and its imprint on the Upper Devonian through Permian stratigraphic record. In: Lucas, S.G., Schneider, J.W., Wang, X., Nikolaeva, S. (Eds.), The Carboniferous Timescale, Geol. Soc. Spec. Publ, vol. 512, pp. 213–245. https://doi.org/10.1144/SP512-2021-124.

Moon, L.R., Judd, E.J., Thomas, J., Ivany, L.C., 2021. Out of the oven and into the fire: Unexpected preservation of the seasonal $\delta^{18}O$ cycle following heating experiments on shell carbonate. Palaeogeogr. Palaeoclimatol. Palaeoecol. 562, 110115. https://doi.org/10.1016/j.palaeo.2020.110115.

Müller, P., Staudigel, P.T., Murray, S.T., Vernet, R., Barusseau, J.-P., Westphal, H., Swart, P.K., 2017. Prehistoric cooking versus accurate paleotemperature records in shell midden constituents. Sci. Rep. 7, 3555. https://doi.org/10.1038/s41598-017-03715-8.

Murray, J., 2010. Mid to Upper Viséan Facies and Palaeoenvironments of the Shannon Basin, Western Ireland. PhD Thesis. University of Dublin, Trinity College, p. 342.

Muscatine, L., Goiran, C., Land, L., Jaubert, J., Cuif, J.P., Allemand, D., 2005. Stable isotopes ($d^{13}C$ and $d^{15}N$) of organic matrix from coral skeleton. Proc. Natl. Acad. Sci. USA 102 (5), 1525–1530. https://doi.org/10.1073/pnas.0408921102.

Nolan, L.S.P., Angiolini, L., Jadoul, F., Della Porta, G., Davies, S.J., Banks, V.J., Stephenson, M.H., Leng, M.J., 2017. Sedimentary context and palaeoecology of *Gigantoproductus* shell beds in the Mississippian Eyam Limestone Formation, Derbyshire carbonate platform, Central England. Proc. Yorks. Geol. Soc. 61 (4), 239–257. https://doi.org/10.1144/pygs2017-393.

O'Donnell, T.H., Macko, S.A., Chou, J., Davis-Hartten, K.L., Wehmiller, J.F., 2003. Analysis of $\delta^{13}C$, $\delta^{15}N$, and $\delta^{34}S$ inorganic matter from the biominerals of modern and fossil *Mercenaria* spp. Org. Geochem. 34, 165–183. https://doi.org/10.1016/S0146-6380(02)00160-2.

Orland, I.J., Burstyn, Y., Bar-Matthews, M., Kozdon, R., Ayalon, A., Matthews, A., Valley, J.W., 2014. Seasonal climate signals (1990–2008) in a modern Soreq Cave stalagmite as revealed by high-resolution geochemical analysis. Chem. Geol. 363, 322–333. https://doi.org/10.1016/j.chemgeo.2013.11.011.

O'Sullivan, G.J., Daly, J.S., Murray, J., Ó'Gogáin, A., Chew, D.M., Drakou, F., Guyett, P. C., Badenszki, E., Hoare, B.C., 2021. Uranium–lead phosphate chronostratigraphy: a proof of concept from the mid-Carboniferous boundary. Sediment. Geol. 422, 105961. https://doi.org/10.1016/j.sedgeo.2021.105961.

Paeckelmann, W., 1931. Die Fauna des deutschen Unterkarbons. Die Brachiopoden. 2: Die Productinae und Productus-ahnlichen Chonetinae. Preuss Geol. Landesanst, p. 440.

Pile, A.J., Young, C.M., 1999. Plankton availability and retention efficiencies of cold-seep symbiotic mussels. Limnol. Oceanogr. 44 (7), 1833–1839. https://doi.org/10.4319/lo.1999.44.7.1833.

Popp, B.N., Anderson, T.F., Sandberg, C.A., 1986. Textural, elemental, 781 and isotopic variations 782 among constituents in Middle Devonian limestones, North America. J. Sediment. Petrol. 56, 715–727.

Posenato, R., Morsilli, M., 1999. New species of *Peregrinella* from the lower cretaceous of the Gargano Promontory (Southern Italy). Cretac. Res. 20, 641–654. https://doi.org/10.1006/cres.1999.0171.

Posenato, R., Crippa, G., de Winter, N.J., Frijia, G., Kaskes, P., 2022. Microstructures and sclerochronology of exquisitely preserved lower Jurassic lithiotid bivalves: Paleobiological and paleoclimatic significance. Palaeogeogr. Palaeoclimatol. Palaeoecol. 602, 111162. https://doi.org/10.1016/j.palaeo.2022.111162.

Poty, E., Devuyst, F.X., Hance, L., 2006. Upper Devonian and Mississippian foraminiferal and rugose coral zonations of Belgium and northern France: a tool for Eurasian correlations. Geol. Mag. 143 (6), 829–857. https://doi.org/10.1017/S0016756806002457.

Pracht, M., Lees, A., Leake, B., Feely, M., Long, C.B., Morris, J., McConnell, B.J., 2004. Geology of Galway Bay: A Geological Description to Accompany the Bedrock Geology, 1:100,000 Scale Map Series, Sheet 14, Galway Bay. Geological Survey of Ireland, p. 76.

Pross, J., Klotz, S., 2002. Palaeotemperature calculations from the Praetiglian/Tiglian (Plio–Pleistocene) pollen record of Lieth, northern Germany: implications for the climatic evolution of NW Europe. Glob. Planet. Chang. 34 (3–4), 253–267. https://doi.org/10.1016/S0921-8181(02)00119-4.

Qiao, L., Shen, S.Z., 2015. A global review of the Late Mississippian (Carboniferous) *Gigantoproductus* (Brachiopoda) faunas and their paleogeographical, paleoecological, and paleoclimatic implications. Palaeogeogr. Palaeoclimatol. Palaeoecol. 420, 128–137. https://doi.org/10.1016/j.palaeo.2014.12.011.

Rau, G.H., Hedges, J.I., 1979. Carbon-13 depletion in a hydrothermal vent mussel: suggestion of a chemosynthetic food source. Science 203 (16), 648–649. https://doi.org/10.1126/science.203.4381.648.

Reynaud-Vaganay, S., Juillet-Leclerc, A., Jaubert, J., Gattuso, J.-P., 2001. Effect of light on skeletal $\delta^{13}C$ and $\delta^{18}O$, and interaction with photosynthesis, respiration and calcification in two zooxanthellate scleractinian corals. Palaeogeogr. Palaeocimatol. Palaeoecol. 175 (1), 393–404. https://doi.org/10.1016/S0031-0182(01)00382-0.

Roark, A., Grossman, E.L., Lebold, J., 2016. Low seasonality in central equatorial Pangea during a late Carboniferous highstand based on high-resolution isotopic records of brachiopod shells. Geol. Soc. Am. Bull. 128 (3–4), 597–608.

Rollion-Bard, C., Garcia, S.M., Burckel, P., Angiolini, L., Jurikova, H., Tomašových, A., Henkel, D., 2019. Assessing the biomineralization processes in the shell layers of modern brachiopods from oxygen isotopic composition and elemental ratios: Implications for their use as paleoenvironmental proxies. Chem. Geol. 524, 49–66. https://doi.org/10.1016/j.chemgeo.2019.05.031.

Rosa, R., Seibel, B.A., 2010. Slow pace of life of the Antarctic colossal squid. J. Mar. Biol. Assoc. U. K. 90, 375–378. https://doi.org/10.1017/S0025315409991494.

Rosa, E.L.M., Vesely, F.F., Isbell, J.I., Kipper, F., Fedorchuk, N.D., Souza, P.A., 2019. Constraining the timing, kinematics and cyclicity of Mississippian–Early Pennsylvanian glaciations in the Parana Basin, Brazil. Sediment. Geol. 384, 29–49. https://doi.org/10.1016/j.sedgeo.2019.03.001.

Rossi, F., Colaco, E., Martinez, M.J., Klein, J.C., Carcaillet, F., Calliere, M.D., De Wit, R., Caro, A., 2013. Spatial distribution and nutritional requirements of the endosymbiont-bearing bivalve *Loripes lacteus* (sensu Poli, 1791) in a Mediterranean *Nanozostera noltii* (Hornemann) meadow. J. Exp. Mar. Biol. Ecol. 440, 108–115. https://doi.org/10.1016/j.jembe.2012.12.010.

Rowley, D.B., Raymond, A., Parrish, J.T., Lottes, A.L., Scotese, C.R., Ziegler, A.M., 1985. Carboniferous palaeogeographic, phytogeographic and palaeoclimatic reconstructions. Int. J. Coal Geol. 5, 7–42.

Rygel, M.C., Fielding, C.R., Frank, T.D., Birgenheier, L.P., 2008. The magnitude of late Paleozoic glacioeustatic fluctuations: a synthesis. J. Sediment. Res. 78 (8), 500–511. https://doi.org/10.2110/jsr.2008.058.

Schöne, B.R., Huang, Q., 2021. Ontogenetic ^{15}N Trends and Multidecadal Variability in Shells of the Bivalve Mollusk, *Arctica islandica*. Front. Mar. Sci. 8, 748593. https://doi.org/10.3389/fmars.2021.748593.

Sevastopulo, G.D., 2009. Carboniferous: Mississippian (Serpukhovian) and Pennsylvanian. In: Holland, C.H., Sanders, I.S. (Eds.), The Geology of Ireland, Second edition. Dunedin Academic Press, Edinburgh, pp. 269–294.

Sevastopulo, G.D., Wyse Jackson, P.N., 2009. Carboniferous: Mississippian (Tournaisian and Viséan). In: Holland, C.H., Sanders, I.S. (Eds.), The Geology of Ireland, Second edition. Dunedin Academic Press Ltd, Edinburgh, pp. 215–268.

Smith, L.B., Read, J.F., 2000. Rapid onset of late Paleozoic glaciation on Gondwana: evidence from Upper Mississippian strata of the Midcontinent, United States. Geology 28, 279–282. https://doi.org/10.1130/0091-7613(2000)28%3C279:ROOLPG%3E2.0.CO;2.

Somerville, H.E.A., 1999. Conodont Biostratigraphy and Biofacies of Upper Visean Rocks in Parts of Ireland. PhD thesis. University College Dublin (National University of Ireland).

Somerville, I.D., Strogen, P., 1992. Ramp sedimentation in the Dinantian Limestones of the Shannon Trough, County Limerick, Ireland. Sediment. Geol. 79, 59–75.

Somerville, I.D., Waters, C.N., Collinson, J.D., 2011. South Central Ireland. In: Waters, C. N., Somerville, I.D., Jones, N.S., Cleal, C.J., Collinson, J.D., Waters, R.A., Besly, B.M., Dean, M.T., Stephenson, M.H., Davies, J.R., Freshney, E.C., Jackson, D.I., Mitchell, W.I., Powell, J.H., Barclay, W.J., Browne, M.A.E., Leveridge, B.E., Long, S. L., McLean, D. (Eds.), A Revised Correlation of Carboniferous Rocks in the British Isles, Geol. Soc. Lon. Spec. Rep, vol. 26, pp. 144–152.

Soreghan, G.S., Giles, K.A., 1999. Amplitudes of Late Pennsylvanian glacioeustasy. Geology 27, 255–258. https://doi.org/10.1130/0091-7613(1999)027%3C0255:AOLPG%3E2.3.CO;2.

Steuber, T., Rauch, M., Masse, J.P., Graaf, J., Malkoč, M., 2005. Low-latitude seasonality of cretaceous temperatures in warm and cold episodes. Nature 437 (7063), 1341–1344. https://doi.org/10.1038/nature04096.

Streel, M., Caputo, M.V., Loboziak, S., Melo, J.H.G., 2000. Late Frasnian–Famennian climates based on palynomorph analyses and the question of the Late Devonian glaciations. Earth Sci. Rev. 52 (1–3), 121–173. https://doi.org/10.1016/S0012-8252(00)00026-X.

Strogen, P., 1988. The Carboniferous lithostratigraphy of southeast County Limerick, Ireland, and the origin of the Shannon Trough. Geol. J. 23, 121–137. https://doi.org/10.1002/gj.3350230202.

Strogen, P., Somerville, I.D., Pickard, N.A.H., Jones, G.Ll., Fleming, M., 1996. Controls on ramp, platform and basinal sedimentation in the Dinantian of the Dublin Basin and Shannon Trough, Ireland. In: Strogen, P., Somerville, I.D., Jones, G.L. (Eds.), Recent Advances in Lower Carboniferous Geology, 107. Geol. Soc. Lon. Spec. Pub., pp. 263–279. https://doi.org/10.1144/GSL.SP.1996.107.01.19

Takayanagi, H., Asami, R., Otake, T., Abe, O., Miyajima, T., Kitagawa, H., Iryu, Y., 2015. Quantitative analysis of intraspecific variations in the carbon and oxygen isotope compositions of the modern cool-temperate brachiopod *Terebratulina crossei*. Geochim. Cosmochim. Acta 170, 301–320. https://doi.org/10.1016/j.gca.2015.08.006.

Tao, K., Robbins, J.A., Grossman, E.L., O'Dea, A., 2013. Quantifying upwelling and freshening in nearshore tropical American environments using stable isotopes in modern gastropods. Bull. Mar. Sci. 89 (4), 815–835. https://doi.org/10.5343/bms.2012.1065.

Tornabene, C., Martindale, R.C., Wang, X.T., Schaller, M.F., 2017. Detecting photosymbiosis in fossil scleractinian corals. Sci. Rep. 7 (1), 9465. https://doi.org/10.1038/s41598-017-09008-4.

Ullmann, C.V., Frei, R., Korte, C., Lüter, C., 2017. Element/Ca, C and O isotope ratios in modern brachiopods: species-specific signals of biomineralization. Chem. Geol. 460, 15–24. https://doi.org/10.1016/j.chemgeo.2017.03.034.

Vermeij, G.J., 2016. Gigantism and its Implications for the history of Life. PLoS One 11 (1), e0146092. https://doi.org/10.1371/journal.pone.0146092.

Viaretti, M., Crippa, G., Brombin, V., Della Porta, G.P., Griesshaber, E., Jurikova, H., Posenato, R., Bottini, C., Angiolini, L., 2025. Duration and intensity of the late Permian (early Wuchiapingian) cool climate episode: Sclerochemical evidence from brachiopod assemblages in Iran. Palaeogeogr. Palaeocimatol. Palaeoecol. 659, 112654. https://doi.org/10.1016/j.palaeo.2024.112654.

Vokhshoori, N.L., Tipple, B.J., Teague, L., Bailess, A., McCarthy, M.D., 2022. Calibrating bulk and amino acid $\delta^{13}C$ and $\delta^{15}N$ isotope ratios between bivalve soft tissue and shell for paleoecological reconstructions. Palaeogeogr. Palaeoclimatol. Palaeoecol. 595, 110979. https://doi.org/10.1016/j.palaeo.2022.110979.

Wright, V.P., Vanstone, S.D., 2001. Onset of late Palaeozoic glacio-eustacy and the evolving climates of low latitude areas: a synthesis of current understanding. J. Geol. Soc. Lond. 158, 579–582. https://doi.org/10.1144/jgs.158.4.579.

Zakowa, H., 1985. Upper Visean gigantoproductoid brachiopods from the Gory Swietokrzyskie, Poland. Annales Societatis Geologorum Poloniae, Krakow 55, 105–126.

Zhang, Z., Augustin, M., Payne, J.L., 2015. Phanerozoic trends in brachiopod body size from synoptic data. Paleobiology 41 (3), 491–501. https://doi.org/10.1017/pab.2015.12.